Involvement of GABAergic interneuron subtypes in 4-aminopyridine-induced seizure-like events in mouse entorhinal cortex in vitro

Paolo Scalmani, Rosina Paterra, Massimo Mantegazza, Massimo Avoli, Marco de Curtis

Involvement of GABAergic interneuron subtypes in 4-aminopyridine-induced seizure-like events in mouse entorhinal cortex *in vitro*

Paolo Scalmani*[1], Rosina Paterra[2], Massimo Mantegazza[3,4,5], Massimo Avoli[6,7] and Marco de Curtis[1]

(1) Epilepsy Unit, Fondazione IRCCS Istituto Neurologico *Carlo Besta*, 20133 Milano, Italy
(2) Molecular Neuro-oncology Unit, Fondazione IRCCS Istituto Neurologico *Carlo Besta*, 20133 Milano, Italy
(3) University Cote d'Azur, 06560 Valbonne-Sophia Antipolis, France
(4) CNRS UMR 7275, Institute of Molecular and Cellular Pharmacology (IPMC), LabEx ICST, 06650 Valbonne-Sophia Antipolis, France
(5) Inserm, 06650 Valbonne-Sophia Antipolis, France
(6) Montreal Neurological Institute-Hospital, McGill University, Montreal, Quebec.
(7) Departments of Neurology & Neurosurgery and of Physiology, McGill University, Montreal, Quebec.

Abbreviated title: Interneurons during focal seizures

The manuscript includes 7 Figures, 3 Extended Data Figures and 1 Tables

Number of pages: 33 **Number of lines**: 796

Words in Abstract 250, Introduction 536 and discussion 2094.

Conflict of interest statement: The Authors declare no conflict of interest.

Acknowledgments: We thank Y. Yanagawa (Gunma University, Japan) for providing GAD67 knock-in mice and G. Szabo (Institute of Experimental Medicine, Budapest, Hungary) for providing GAD65 transgenic mice. The study was supported by grants from the Italian Ministry of Health (Current Research

2021 and Grant RF 2018-12365681). the Paolo Zorzi Association for Neuroscience (2021-24 EPICARE project) and the Canadian Institutes of Health Research (PJT153310 and PJT166178) to Massimo Avoli.

(*) Correspondance to Paolo Scalmani, Fondazione IRCCS Istituto Neurologico *Carlo Besta*, 20133 Milano, Italy. Email *paolo.scalmani@istituto-besta.it*

Abstract

Single unit recordings performed in temporal lobe epilepsy patients and in models of temporal lobe seizures have shown that interneurons are active at focal seizure onset . Here we performed simultaneous patch clamp and field potential recordings in entorhinal cortex slices of GAD65 and GAD67 mice that express green fluorescent protein in GABAergic neurons, to analyze the activity of specific interneuron (IN) subpopulations during acute seizure-like events (SLEs) induced by 100 µM 4-aminopyridine. IN subtypes were identified as parvalbuminergic (IN_{PV}; n=17), cholecystokinergic (IN_{CCK} n=13) and somatostatinergic (IN_{SOM} n=15) according to neurophysiological features and single cell digital PCR.

IN_{PV} and IN_{CCK} discharged at the start of 4AP-induced SLEs that were characterized by either low-voltage fast or hyper-synchronous onset pattern; IN_{SOM} were active >100 ms ahead of SLEs while pyramidal neurons become active with variable delays after SLE onset. Depolarizing block was observed in about 50% of cells in each IN subgroup and it was longer in IN (*circa* 4 sec) than in pyramidal neurons (<1 sec). As SLE evolved, all IN subtypes generated action potential bursts synchronous with the field potential events leading to SLE termination. High frequency firing throughout the SLE occurred in one third of IN_{PV} and IN_{SOM}.

We conclude that entorhinal cortex INs are very active from the very onset and during the progression of SLEs induced by 4AP. These results, which support earlier *in vivo* and *in vivo* evidence, show that IN play an active role in the initiation and the development of focal seizures.

Abbreviations

4-aminopyridine = 4AP; action potential = AP; after-hyperpolarizing potential = AHP; modified artificial cerebrospinal fluid = ACSF; parvalbumin = PV; cholecystokinin = CCK; somatostatin = SOM; depolarizing block = DB; entorhinal cortex = EC; green fluorescent protein = GFP; hypersynchronous = HYP; I/O = input-output; interneurons = IN; pyramidal neurons = PYR; local field potential = LFP; low-voltage fast = LVF; Maximum decay slope = MDS; maximum rise slope = MRS; **picrotoxin = PTX;** reverse transcription = RT; seizure-like event = SLE; single cell digital PCR = sc-dPCR; temporal lobe epilepsy = TLE.

Introduction

Clinical and experimental studies have provided evidence for distinctive and region-specific network mechanisms associated with the onset of focal seizures (Perucca and O'Brien, 2015; Singh et al., 2015; Lagarde et al., 2016; Uva et al., 2017b; Devinsky et al., 2018; Di Giacomo et al., 2019; Gnatkovsky et al., 2019). Reproducible seizure patterns described in patients with temporal lobe epilepsy (TLE), have been replicated in *in vitro* preparations and in TLE animal models, to identify network and cellular processes responsible for their generation and progression (Avoli et al., 2016; De Curtis and Avoli, 2016). Two seizure onset patterns were observed in TLE patients during pre-surgical monitoring with intracranial EEG electrodes (low-voltage fast – LVF- and hypersynchronous - HYP; Engel, 1990); these two onset patterns were confirmed in rodent TLE-HS models (Grasse et al., 2013; Lévesque et al., 2013; Bragin et al., 1999; Riban et al., 2002). Moreover, *in vitro* experiments performed in rodent brain slices (Lopantsev and Avoli, 1998a; Derchansky et al., 2008; Losi et al., 2010; Zhang et al., 2012; Lévesque et al., 2013; Behr et al., 2014; Avoli et al., 2016; Codadu et al., 2019) or in the isolated whole guinea pig brain (Uva et al., 2005; Boido et al., 2014b) confirmed the occurrence of LVF and HYP seizure onsets during application of convulsive drugs. Specifically, in entorhinal cortex slices that were perfused with a solution containing the potassium channel blocker 4-aminopyridine (4AP), LVF seizures correlated with the activation of interneuronal networks (Lopantsev and Avoli, 1998a; Avoli et al., 2016). In the same model, HYP seizures were shown to be associated with interneuron discharges (Derchansky et al., 2008) and prominent GABAergic post-burst hyperpolarizations that progressively decrease in amplitude while unrestrained excitation enhances as seizure activity develops (Zhang et al., 2012; Avoli et al., 2016; Köhling et al., 2016).

Interestingly, *in vitro* experiments during 4AP application have shown that optogenetic activation of GABAergic interneurons **(INs)** induced SLEs with LVF-onset HYP seizure onset pattern occurred when principal cells were optogenetically stimulated thus suggesting that both types of seizure onset patterns can be generated under identical conditions by activating specific neuronal subpopulations (Shiri et al., 2016). The involvement of entorhinal cortex (EC) interneurons in SLEs induced by 4AP (and by other compounds) were confirmed by intracellular recordings performed on the guinea pig isolated brain (Gnatkovsky et al., 2008; Uva et al., 2015) and by single unit recordings of putative INs in EC slices with tetrode wires

(Lévesque et al., 2018). Interneuron activity, and the resulting GABA release, leads to massive activation of post-synaptic $GABA_A$ receptors, which favors seizure generation through intracellular accumulation of Cl^- and the subsequent increase in extracellular $[K^+]$ due to activation of the K^+-Cl^- cotransporter-2 (Avoli et al., 1996b, 1996a; Librizzi et al., 2017; Di Cristo et al., 2018). Moreover optogenetic photostimulation of PV and SOM IN evokes epileptiform discharges similar to those occurring spontaneously during 4AP application in cortical slices (Yekhlef et al., 2015; Shiri et al., 2016). Overall, these findings indicate that SLEs generated *in vitro* by cortical networks during 4AP treatment are caused by enhanced interneuron activity. Therefore, in this study, we evaluated the participation of different subpopulation of GABAergic INs to the initiation and maintenance of SLEs induced by 4AP in mouse EC slices.

Methods

Animal care and mouse lines. Experiments were carried out on C57BL/6J mice (Charles River, Calco, Italy, https://www.criver.com/products-services/find-model/jax-c57bl6j-mice?region=27) according to the European directive 2010/63/UE, approved by institutional and national ethical committees (Protocol 711/2016-PR). All efforts were made to minimize the number of animals and their suffering. Mice were group housed (5 per cage, or 1 male and 2 females per cage for breeding) on a 12 h light/dark cycle, with *ad libitum* supply of water and food.

Entorhinal cortex brain slices. Brain slices were prepared as previously described (Mantegazza et al., 1998; Aracri et al., 2006) from 20 to 30 day- old C57BL/6J mice that selectively express the green fluorescent protein (GFP) in GABAergic IN specifically: GAD65-GFP transgenic mice (López-Bendito et al., 2004) and GAD67-GFPΔneo knock-in mice (Tamamaki et al., 2003). **GAD67 knock-in mice were provided by Y. Yanagawa (Gunma University, Japan), GAD65 transgenic mice were provided by G. Szabo (Institute of Experimental Medicine, Budapest, Hungary).** Animals were killed by decapitation under isofluorane anesthesia, the brain was quickly removed and placed in ice-cold modified artificial cerebrospinal fluid (mACSF), which contained (mM): 87 NaCl, 7 $MgCl_2$, 2.5 KCl, 0.5 $CaCl_2$, 21 $NaHCO_3$, 1.25 NaH_2PO_4, 25 glucose and 75 sucrose. mACSF was bubbled with 95% O_2 5% CO_2. Horizontal slices (400 µm thick) that contained the ventral hippocampus and the entorhinal cortex were cut with a vibratome (Leica VT1200S;

Wetzlar, Germany) in ice-cold mACSF and were placed in an incubation chamber bathed in standard ACSF at room temperature, which contained (mM): 129 NaCl, 1.8 $MgSO_4$, 3 KCl, 1.6 $CaCl_2$, 21 $NaHCO_3$, 1.25 NaH_2PO_4 and 10 glucose.

Electrophysiological recordings. Electrophysiological recordings started after an incubation/recovery period of at least one hour. One slice at the time was transferred in the recordings chamber (Warner INtruments, Hamden, CT, US) and GFP-fluorescent IN were visualized by infrared video microscopy with a Nikon Eclipse FN1 microscope (Nikon, Minato, Japan) equipped with DIC optics and a CCD camera (Hamamatsu, Japan). Simultaneous extracellular local field potential (LFP) and whole-cell, current-clamp patch-clamp recordings (LFPe and PCe electrodes in Extended Data Fig. 1-1A) were performed at 25°C with Multiclamp 700B patch-clamp amplifier, Digidata 1440a digitizer and pClamp 10.2 software (Axon Instruments-Molecular Devices, San Jose, CA, US). Pipettes were pulled (Sutter Instruments, Novato, CA, US) from borosilicate glass capillaries to a resistance of 2.5-3.0 MΩ (access resistance of 4-7 MΩ). The internal pipette solution for LFP recordings was mACSF while for current-clamp patch-clamp recordings it contained (in mM): 120 K-gluconate, 15 KCl, 2 $MgCl_2$, 0.2 EGTA, 10 HEPES, 2 Na_2ATP, 0.2 Na_2GTP, 20 P-creatine, RNAse inhibitor (AM2682, 0.5 U/µl, Invitrogen,Weltham, MA, US), pH 7.2 with KOH. For LFP recordings we used the Multiclamp 700B amplifier in I=0 mode; for whole-cell recordings we used it in current-clamp mode maintaining, after appropriate bridge balance compensation, the cell resting membrane potential at -70 mV by intracellular current injection. Whole-cell patch-clamp recordings were performed from the cell soma; IN were identified by GFP fluorescence (red arrow in Extended Data Fig. 1-1C), pyramidal neurons (PYR) were identified by their size and the pear-like appearance of the soma and by the lack of GFP fluorescence (black arrow in Extended Data Fig. 1-1B). Signals were filtered at 10 kHz and were sampled at 50 kHz. Signal analyses were performed using pClamp 10.5 and Origin 8.5 pro (Origin Lab, Northampton, MA, US).

Input-output curves were obtained by injecting 2.5-sec depolarizing current pulses, which were increased by 10 pA steps (Fig. 1A and B). Action potential (AP) firing adaptation was measured quantifying inter-spike intervals between subsequent APs elicited by current pulses inducing depolarization ranging between 2 and 5 mV above AP firing threshold. **In adapting neurons, the AP interval was short at**

the beginning of depolarizing pulse-induced AP firing and long at the end of recording. Neurons with unstable resting potential and/or unstable firing patterns were discarded from the analysis.

Quantitative evaluation of AP dynamic changes was performed by phase plot analysis (Jenerick, 1963; Bean, 2007). The first derivative of the action potential (dV/d*t* measured as mV/ms; *y*-axis in Fig. 1C and dotted line in Extended Data Fig. 1-2A) were plotted against the Instantaneous membrane potential (measured in mV; *x*-axes of Fig. 1C and continuous line in Extended Data Fig. 1-2A). AP features are represented as a loop in which the rising starting point represents the AP threshold ($V_{threshold}$ in Extended Data Fig. 1-2B), the extreme right value is the maximal voltage amplitude (V_{peak}), the upper and lower peaks of the loop are the maximum rise slope (MRS) and the maximum decay slopes (MDS), respectively. Phase plot loops were smoothed with an Origin SP-line function. Phase plot analysis magnifies and highlights $V_{threshold}$, V_{peak}, MRS and MDS changes (arrows in Extended Data Fig. 1-2B). Mean phase plots (Fig. 1 C) were constructed by aligning the AP peak (continuous line in Extended Data Fig. 1-2A) to the first derivative peak (black dotted line) for each cell; the obtained curves were further aligned by placing the peaks of the APs at the zero y point of the first derivative as shown in Extended Data Fig. 1-2A (red dotted line); average errors were reported on phase plot x axis (membrane potential) and y axis (slope) in Fig. 1C. The graphs in Extended Data Fig. 1-2B were constructed on average curves aligned to the AP peak. SLEs were induced perfusing brain slices with freshly made ACSF with low Mg^{2+} (0.5 mM) and 100 µM 4AP (Sigma A78403).

Single-cell reverse transcription and digital PCR. For single-cell digital PCR (sc-dPCR), a gentle negative pressure was applied to the patch pipette after completing the electrophysiological recording to harvest the cell cytoplasm containing RNA. The intracellular material pulled in the electrode (5 µl) was placed in a test tube (cat. AB-0620, Thermo Fisher Scientific, Waltham, MA, US) for short treatment with DNAase and then for reverse transcription (RT) using the SuperScript IV VILO Master Mix with exDNase enzyme (Thermo Fisher Scientific cat. 11766050). The RNA from each individual cell was subjected to gDNA digestion at 37°C for 2 minutes in a total volume of 10 µl (gDNA digestion reaction mix: 1 µl ezDnase enzyme, 1 µl ezDNase Buffer RNA to 10 µl in Rnase free H_20), it was briefly centrifuged and placed on ice, and then reverse transcribed in a total volume of 20 µl (4 µl Super Script IV VILO Master Mix, 6 µl nuclease free water, 10 µl gDNA digested RNA). RT was carried out with subsequent cycles at 25°C for 10 minutes, at 50°C for 10 minutes and at 85° for 5 minutes. The material was finally stored at -80°C until preamplification.

Digital PCR was carried out after cDNA preamplification in a 30 µl TaqMan® PreAmp Master Mix (Thermo Fisher Scientific; cat. 4384267), 15 µl Pooled TaqMan® Gene Expression Assays (0.2X) and 15 µl cDNA. For the assay pool, equal volume of each 20x TaqMan® Gene expression Assay was combined (Thermo Fisher Scientific; see Table.1) at a final concentration of 0.4x per assay. PreAmp cycling protocol: 10 min enzyme activation at 95°C followed by 10 denaturation cycles at 95°for 15 sec and annealing at 60°C for 4 minutes followed by 10 minutes at 99°C for enzyme inactivation and hold at 4°C. In each preamplification session a No Template Control was always inserted and the same was then used as a negative control in the dPCR. After preamplification, sc-dPCR was carried out in a Quant Studio 3D Digital PCR System (Thermo Fisher Scientific, detection channels FAM/SybrGreen, VIC, ROX). Both target and reference gene were run in duplex, each dPCR chip was load with 16 µl reaction mix containing 6 µl preamplified PCR mixture, 8 µl Master Mix (Quant Studio 3D Master Mix V2, Thermo Fisher Scientific cat. A26358), 0.8 µl endogenous control assay (*Gapdh*_VIC 20x), 0.8 µl target gene assay (*Pv/Cck/Som*) and 0.4 µl nuclease free water. For each cell, 5 chips were loaded, one for each target. The dPCR chips were loaded into ProFlex PCR System (Thermo Fisher Scientific) for 10 min at 96°C, 2min at 60°C and 30 sec at 98°C for 45 cycles, then 2min at 60°C and hold at 10°C. The chips were read on QuantStudio™3D Digital PCR System and data were processed with Quant Studio™ 3D Analysis Suite (Thermo Fisher Scientific). For each cell, the statistical analysis (Fig. 2 A-C) was obtained by equaling the sum of the copies/ul of each target at 100 and the individual targets as a percentage of the total.

Statistics. Statistical analysis was performed using Prism 6.0 software (GraphPad, San Diego, CA, US) or Origin2021 (OriginLab); The Fisher Exact test with Bonferroni's correction was used for the data expressed as percentage (Fig 1E and Extended Data Fig. 1-1D); ANOVA one-way test for normally distributed data with Tukey 's multiple comparison and Kruskal Wallis test with multiple comparison Dunn's test were used for data not normally distributed. T-test and Wilcoxon Mann Whitney test were used for single population data distributed either normally or not, respectively (Fig. 4); comparison of actual and expected frequencies for categorical data were obtained with the Chi-Square "Goodness of Fit" test.

Results

Our study was based on simultaneous extracellular LFP recordings and intracellular patch-clamp recordings that were performed from 45 IN and 10 PYR in 55 horizontal EC slices; 33 and 22 cells were recorded from superficial and deep EC layers, respectively (Extended Data Fig. 1-1E). In 7 additional EC slices, the effects of receptor antagonists were analyzed during extracellular LFP recordings (see below)

Interneuron subtypes. Based on both firing and AP properties, we grouped IN in four subtypes, which are described below (Fig. 1A-C). We identified 17 presumed parvalbuminergic IN (IN_{PV}; red traces and symbols throughout the manuscript) that typically generated APs that were followed by pronounced after-hyperpolarizing potentials (AHPs; asterisks in Fig. 1A left panel) (Kecskes et al., 2020; Fernandez et al., 2022, Andrew Younget al., 2009). IN_{PV} sustained high frequency AP firing up to 60 Hz and demonstrated a linear average current/voltage relationship (I/O plots in Fig. 1B) with no frequency rate adaptation just above firing threshold (red dots in Fig. 1D). Moreover, as reported in previous studies (Goldberg et al., 2008; Helm et al., 2013; Miyamae et al., 2017) all IN_{PV} showed a delay in the AP onset following injections of current just above AP threshold (arrowheads in Fig. 1A). Phase plot analysis demonstrated two accelerations in the AP rising phase (arrowheads in Fig. 1C; Extended Data Fig. 1-2B). IN_{PV} showed a higher AP threshold compared to IN_{CCK} (Extended Data Fig. 1-2C) and a lower MRS than $IN_{SOM4/5}$ and PYR (Extended Data Fig. 1-2E). In all putative IN_{PV} in which sc-dPCR was performed (11 out of 17 IN_{PV} identified by intrinsic electrophysiological properties) the presence of cDNA for PV was confirmed (red dots in Fig. 2A). Interestingly, a subpopulation of IN_{PV} cells also co-expressed CCK (Fig. 2A, green dots) and SOM (dark blue dots in Fig. 2A; see Discussion). Firing and AP properties were not different in IN_{PV} recorded in superficial or deep EC layers.

Presumed cholecystokininergic IN (IN_{CCK}; n=13; green traces and drawings) responded with a burst of APs to threshold firing depolarization (arrows on green trace of the sec row in Fig. 1A). As previously reported (Varga et al., 2010; Armstrong et al., 2016), IN_{CCK} I/O relationship showed a lower rate of maximum discharge (approx. 40 Hz) during depolarizing pulse injections compared to IN_{PV}. Most IN_{CCK} (92.3%) showed an initial AP adaptation (upper green trace in Fig. 1A, green dots in Fig. 1E) and the rising AP slope showed a single acceleration phase (Fig. 1C; Extended Data Fig. 1-2B). In 77% of IN_{CCK} we observed a

decrease in AP amplitude starting from the second AP of the discharge (arrow on the first row in Fig. 1A), (Karson et al., 2009; Goff and Goldberg, 2019). As for IN_{PV}, IN_{CCK} showed a lower MRS compared to $IN_{SOM4/5}$ and PYR (Extended Data Fig. 1-2E). Sc-dPRC performed in 12 out of 13 IN_{CCK} confirmed CCK cDNA in all cells (green dots Fig. 2B). In 8 IN_{CCK}, cDNA for PV and SOM was also found (red and blue dots in Fig. 2B). Firing properties were not different in IN_{CCK} recorded from superficial and deep EC layers.

IN_{SOM} features have been described in the EC (Neske et al., 2015; Ferrante et al., 2017; Kecskés et al., 2020; Fernandez et al., 2022). In line with Neske et al. (2015)), two different types of presumed somatostatinergic cells (IN_{SOM}) were recorded in superficial and deep EC layers: (i) superficial layer $IN_{SOM2/3}$ (n= 6; light blue in the middle column of Fig. 1A-C) featured slowly adapting APs (light blue dots in Fig. 1D and E) without AHP. and (ii) a single-phase AP acceleration (Fig. 1C and Extended Data Fig. 1-2B); deep layer $IN_{SOM4/5}$ (n= 9; blue in Fig. 1A-C) showed fast rising non-adapting APs that sustained very high firing rate (>100 Hz) during injection of large amplitude depolarizing current steps. APs in $IN_{SOM4/5}$ were followed by fast AHPs (asterisk on blue trace in Fig. 1A). Unlike $IN_{SOM2/3}$, deep layer $IN_{SOM4/5}$ featured a double AP slope acceleration (arrowheads in Fig. 1C, Extended Data Fig. 1-2B). Finally, $IN_{SOM4/5}$ showed a significantly greater MRS than IN_{PV}, IN_{CCK} and PYR (Extended Data Fig. 1-2E) and a significantly faster repolarization compared to all IN subtypes and PYR (Extended Data Fig. 1-2F). Sc-dPCR demonstrated SOM cDNA in IN_{SOM} of both superficial and deep layers (n=12 IN_{SOM}), with minor content of both PV and CCK cDNA (red and green dots in Fig. 2C).

PYR neurons (n=10; black lines and drawings in Extended Data Fig. 1A-C) typically generated adapting APs (Fig. 1A, 2A and B) with no AHP and showed maximal firing rate below 20 Hz. Average maximal AP amplitude in PYR was significantly higher in comparison to all IN (Fig. 1C and Extended Data Fig. 1-2D).

Since sc-dPCR showed higher cDNA copies of CCK than PV in 4 out of 11 IN_{PV}, we further analyzed electrophysiological features in these 4 IN_{PV} (Extended Data Fig. 2-1). I/O curves, AP adaptation features, and AP phase plots of these 4 IN_{PV} (purple dots in Extended Data Fig. 2-1 A-B and purple line in Extended Data Fig. 2-1C) were identical to the other IN_{PV} cells (red dots and line) and were different from IN_{CCK} (green dots and line). As shown in Extended Data Fig. 1-1D, most IN recorded from GAD67 mice were either IN_{SOM} (100%) or IN_{PV} (85.7%), whereas fluorescent IN in slices from GAD65 mice were mainly

(83.33%) IN_{CCK}. The percentage of IN_{PV}, IN_{CCK} and IN_{SOM} recoded in superficial layers (2 and 3) or deep layers (4 and 5) of the EC are illustrated in Extended Data Fig. 1-1E.

Activity of interneurons and pyramidal cells during 4AP-induced epileptiform discharges. Simultaneous extracellular and intracellular IN recording were performed in control conditions and during perfusion with medium containing 100 µM 4AP, which induced in all slices SLEs. Interestingly, during 4AP application all recorded IN were very active before and during all phases of SLEs. In all IN, subthreshold spontaneous activity was observed during 4AP perfusion (arrowheads in Fig. 3A, C and D) in parallel with an increased background activity observed in the LFP recording (Fig. 3D). **As commonly observed in brain slices in control conditions, INs show no or very sporadic AP firing before 4AP (control condition, upper panel in Fig. 3E); within 10 minutes after 4AP perfusion onset, AP firing was observed in 78.2% IN during the pre-SLE period (lower panel in Fig 3E). In** the 180 sec before SLE onset, pre-ictal AP firing was observed in 13 out of 17 IN_{PV} (red dots in Fig. 3E), in 9 out of 13 IN_{CCK} (green dots) and in 10 out of 15 IN_{SOM} (blue dots). Interictal APs superimposed to large amplitude synaptic event was observed in 7.5% IN_{PV}, in 92.3% IN_{CCK} (example in Fig. 3A and D) and 80% IN_{SOM}, respectively. Virtually, all IN were entrained during SLEs (96%). Unlike IN, PYR showed neither enhanced synaptic activity nor spontaneous firing during 4AP before SLEs (Fig. 3B; black dots in Fig. 3E).

Field potential pre-ictal spikes were observed ahead of SLEs in all experiments; virtually all IN generated either single APs or AP burst that were superimposed on a depolarizing potential and correlated with these field preictal spikes (Fig. 3A, C and D). The 4AP-induced pre-ictal epileptiform discharges recorded with extracellular fields in a subset of experiments (n= 7) were not modified by co-perfusion with either 3 mM kynurenic acid (a **broad spectrum glutamatergic antagonist,** n = 4) or 10 µM DNQX **(a selective non-NMDA glutamatergic antagonist)** + 10 µM d-CPP (a **competitive NMDA antagonist,** n= 3,) and were abolished by 4AP co-perfusion with 100 µM $GABA_A$ receptor blocker, picrotoxin (**PTX**; n= 7; representative example in **Fig. 4A**). **In addition, interictal spikes were generated during co-perfusion of 100 µM 4AP and 100 µM PTX (arrowheads in Fig. 4B), but SLEs were not observed (n=9). Reperfusion of 4AP after PTX washout (right part of Fig. 4B) promoted an increase of background**

synaptic noise (which was occluded by the simultaneous PTX+4AP perfusion) that culminated with a SLE (n=7).

In line with previous reports (Boido et al., 2014b; Avoli et al., 2016), 4AP-induced SLEs were characterized by two main types of field potential onset: SLEs with extracellular LVF activity (representative example in Fig. 3A; n=29) and SLEs with large amplitude extracellular spikes at onset (HYP; arrows in Fig. 3C; n=15). Extracellular recordings confirmed that both LVF and HYP SLEs were superimposed to a large amplitude, negative slow potential deflection likely due to changes in extracellular potassium concentration (Avoli et al., 1996a, 1996b; Gnatkovsky et al., 2008; Librizzi et al., 2017). All recorded IN were active from the very onset of both SLE types. LVF onset SLE patterns were recorded in 70.6% IN_{PV}, 54% IN_{CCK}, 50% IN_{SOM} and 80% PYR; HYP SLE onset patterns were recorded in 29.4% IN_{PV}, 46% IN_{CCK},50% IN_{SOM} and 20% PYR.

Next, we analyzed the temporal correlation between LFP onset of SLE and the activity of PYR and IN subtypes. As illustrated in Figure 5A, we utilized two measures to evaluate the delay between neuronal activity and the extracellular discharge. **First, we calculated the delay between the onset of extracellular fast activity in LVF onset or the first burst spike in HYP onset SLEs and the first AP of the ictal discharge (parameter *a* in the expanded trace of Fig. 5A). The second parameter was the delay between the first intracellular depolarizing potential recorded at SLE onset and the initiation of the slow deflection in both LVF and HYP extracellular SLEs (parameter *b* in Figure 5A). Figure 5B show that both delays *a* and *b* were negative or close to zero for all IN subtypes and were positive in most PYRs (see Figure 5 legend), demonstrating a delayed PYR firing with respect to extracellular SLE onset. As illustrated in Figure 5C for parameter *b*, most $IN_{SOM4/5}$, $IN_{SOM2/3}$ and IN_{CCK} fired action potentials before the extracellular SLE (time 0) while IN_{PV} became active just before or after the extracellular the SLE onset. Statistical analysis showed that IN_{SOM} activity consistently started before PYR (asterisks on the right of box chart in Fig. 5Bb).** These data demonstrate that during both LVF and HYP SLEs induced by 4AP in the mouse EC, IN_{SOM} are active before PYR. These findings also suggest that PYR activity follows IN_{CCK}, IN_{SOM} and IN_{PV} activities at SLE discharge onset.

During SLEs, depolarizing blockade (DB; arrowhead in Fig. 6A) of AP firing was observed in 37.5% IN_{PV}, in 50% IN_{CCK}, in 44.4% IN_{SOM} and in 40% PYR (Fig. 6B). DB was observed at the beginning of both LVF

297 and HYP SLEs and lasted 4.56 ± 1.36 sec, 3.97 ± 2.20 sec, and 3.64 ± 1.06 sec in IN_{PV}, IN_{CCK}, and IN_{SOM},
298 respectively (Fig. 6D). Compared to IN, DB duration in PYR was shorter (0.95 ± 0.19 sec; Fig. 6D). DB was
299 consistently observed only in IN and PYR in which membrane potential depolarized above -30 mV during
300 SLE onset (Fig. 6C). As SLEs progressed, firing resumed after DB in all IN subtypes. During the last phases
301 of the SLEs, sustained AP firing was consistently observed in all IN and PYR. Except for a subgroup of IN
302 (see below), intracellular bursting activity was synchronized with the LFP bursting observed during the late
303 stage of SLEs (Aracri et al., 2006; Boido et al., 2014a).

304 **We identified three different seizure end patterns that** are illustrated in Fig. 7A and quantified in the
305 graph in Fig. 7B. Short AP bursts synchronous to the LFP burst (Fig. 7Aa and black columns in Fig. 7B)
306 were prominent in PYR (66.66%), were present in 25% of IN_{SOM} and were sporadically observed in IN_{PV}
307 (9%) and IN_{CCK} (7.6%). Virtually all IN_{CCK} generated a robust bursting discharge that extended beyond the
308 duration of the simultaneously recorded extracellular burst discharge (Fig. 7Ab and striped columns in Fig.
309 7B). This type of pattern was observed also in 54.5% IN_{PV}, 41.66% IN_{SOM} and 33.34% PYR. Finally, high
310 frequency firing was observed exclusively in IN_{PV} (36.5%) and IN_{SOM} (36.34 %; Fig. 7Ac and empty
311 columns in Fig. 7B); a burst discharge synchronous with the LFP burst was nested within the high frequency
312 barrage (Fig. 7Bc). Interestingly, DB was observed also in 1 out of 6 IN_{PV} and 2 out of 4 IN_{SOM} that
313 displayed a continuous high frequency firing. Late bursting patterns were observed in both LVF and HYP
314 SLEs.

315

316 **Discussion**

317 The present study provides new evidence for the role of different IN subpopulations in the generation of
318 seizure-like discharges induced by acute 4AP treatment in the *in vitro* mouse EC slice preparation. Our
319 findings demonstrate that 4AP-induced SLEs: i) are preceded by enhanced IN firing leading to GABAergic
320 pre-ictal spikes**, ii) are abolished by co-perfusion of 4AP with the GABA receptor antagonist picrotoxin,**
321 **iii)** initiate with the activation of IN_{PV}, IN_{CCK} and IN_{SOM}, followed by the recruitment of PYR, and **iv)** are
322 characterized by intense involvement of all IN subtypes throughout their development and termination.

Early studies have reported that the onset of SLEs induced by 4AP in EC slices is associated to a synchronous field potential that likely mirrors IN activity (Avoli et al., 1993, 1996a; Lopantsev and Avoli, 1998b). These results were later confirmed and were reproduced in several experiments, including hippocampal and EC slices from different rodents and the isolated guinea pig brain preparation (for review see Avoli & de Curtis 2011; Avoli and de Curtis, 2011; Kaila et al., 2014; De Curtis and Avoli, 2016; Devinsky et al., 2018). SLEs initiation by IN was confirmed in neocortex, hippocampus and EC *in vitro* after exposure to 4AP (Gnatkovsky et al., 2008; Uva et al., 2009, 2015, 2017a; Avoli et al., 2016; Librizzi et al., 2017; Lado et al., 2022) low bicuculline concentration (Gnatkovsky et al., 2008; Uva et al., 2015) and low-Mg^{2+}/high-K^{+} solution (Dzhala and Staley, 2003; Ziburkus et al., 2006; Lasztóczi et al., 2009) as well as d following high frequency stimulation (Kaila et al., 1997; Perez Velazquez and Carlen, 1999; Fujiwara-Tsukamoto et al., 2007). These studies indicate that GABAergic network hyperactivation is common at the onset of *in vitro* SLEs generated acutely following diverse experimental manipulations and it is thus not observed only during 4AP treatment.

IN activity at seizure onset was confirmed by single and multiunit *in vivo* recordings performed models of temporal lobe epilepsy (Grasse et al., 2013; Fujita et al., 2014; Toyoda et al., 2015) and in patients with focal epilepsies (Truccolo et al., 2011; Elahian et al., 2018; Weiss et al., 2019; Merricks et al., 2021). Interestingly, hyperactivity of GABAergic neurons is also involved in the initiation of other pathological network activities, such as migraine-related cortical spreading depolarization (Chever et al., 2021; Lemaire et al., 2021)

The 4AP focal seizure model. The 4AP *in vitro* model has been employed to study cellular seizure mechanisms in temporal lobe structures. 4AP induces SLEs with electrographic features typical of human LVF or HYP seizure onset patterns. Similar electrographic features were obtained also by systemic 4AP treatment *in vivo* (Lévesque et al., 2013) and by perfusing 4AP in the *in vitro* isolated guinea pig brain preparation. At present, details on IN firing properties and IN phenotypes cannot be achieved with *in vivo* recording in chronic models of epilepsy, such as the pilocarpine or kainic acid TLE models. Our study analyzed 4AP-induced network activities on naïve EC-hippocampal slices obtained from non-epileptic animals. The use of *in vitro* slices from chronically epileptic animals could be considered a better option to

analyze the microcircuitry involved in SLEs generation. However, *in vitro* brain slices do not generate seizures spontaneously: this aspect makes the use of brain tissue slices from chronic TLE animals impractical to analyze cellular network interactions during SLEs, since pro-epileptic drugs would be, in any case, necessary to induce epileptiform discharges. This is an intrinsic limitation of *in vitro* experimental studies of ictogenesis that cannot be bypassed.

GABAergic interneuron phenotyping. We utilized EC slices obtained from GAD65 or GAD67 mice, which express GFP exclusively in GABAergic interneurons (Tamamaki et al., 2003; López-Bendito et al., 2004). Several studies demonstrated that cortical IN can be identified by electrophysiological features (Freund and Buzsáki, 1996; Kawaguchi and Kondo, 2002; Rudy et al., 2011; Urban-Ciecko and Barth, 2016; Pelkey et al., 2017). IN_{PV}, IN_{CCK} and IN_{SOM} firing features described in rodent EC (Varga et al., 2010; Neske et al., 2015; Armstrong et al., 2016; Ferrante et al., 2017; Fernandez et al., 2022) are similar to those reported for other cortical areas and for the hippocampal region (Pelkey et al., 2017). Parameters usually considered as reliable for IN phenotyping include AP features, firing discharge and adapting properties. We classified the recorded IN according to these criteria. Another IN marker is the cDNA content revealed by sc-dPCR. We demonstrated here that IN contain different amounts of PV and CCK cDNA. This co-expression most likely reflects the high sensibility of digital PCR technique.

Studies that utilized single-cell reverse transcription-polymerase chain reaction techniques have shown that *circa* 30–40% of cortical IN express CCK cDNA (Gallopin et al., 2006), It is however debated whether transcript expression reflects CCK-GABA neuron identity (Tricoire et al., 2011). As reported in Extended Data Fig. 2-1, IN with high PV and CCK co-expression were classified as IN_{PV} based on membrane and firing properties. Our analysis demonstrates that the electrophysiological characterization is the most reliable identifier to stratify IN subtypes. Of note, IN clustering according to electrophysiological criteria showed that the variability of both input-output curve and average phase plots values were minimal, as shown in Fig. 1B and C, suggesting a high homogeneity of firing patterns within each identified IN subgroup.

Interneuron activity during pre-ictal and SLE dynamics. IN subtypes have been studied in the EC and in the hippocampus (Tremblay et al., 2016; Pelkey et al., 2017). IN_{PV} form perisomatic contacts with principal cells broadly distributed throughout EC layers (Beed et al., 2013; Couey et al., 2013; Fuchs et al., 2016;

Kecskés et al., 2020) by targeting the soma and the spike initiation zone, these cells are in a unique position to control the occurrence and the timing of postsynaptic cell AP firing. IN_{SOM} and some IN_{CCK} preferentially target dendrites of principal neurons with higher density in layers III-V (Fuchs et al., 2016; Tremblay et al., 2016; Kecskés et al., 2020), where they are proposed to gate and modulate excitatory inputs (Urban-Ciecko and Barth, 2016). While IN_{CCK} have not been specifically studied in the EC, it is well known that they form synaptic contacts both in the soma and in apical dendrites of postsynaptic principal cells in neocortex (Nguyen et al., 2020). Interestingly, EC IN_{PV} are interconnected through reciprocal synaptic interactions and gap junctions (Hjorth et al., 2009; Fernandez et al., 2022). IN_{PV} and IN_{SOM} are also synaptically connected in the hippocampus (Karson et al., 2009). Moreover, IN_{SOM} are coupled via gap junctions with other IN, but not with other IN_{SOM} (Pfeffer et al., 2013; Fernandez et al., 2022). These intra-IN connectivity forms functional interactions that are crucial to sustain GABAergic neuronal network activity, including neuronal oscillations (Klausberger et al., 2005; Cardin et al., 2009) and likely focal seizures.

We demonstrated here that background firing and GABAergic synaptic activity during 4AP application is enhanced in IN, but not in PYR. Accordingly, pre-ictal spiking activity induced by 4AP was blocked by GABAergic antagonists, but not by glutamatergic receptor antagonists (Uva et al., 2013). Since we observed enhanced synaptic activity exclusively in IN, we assumed that increased spontaneous synaptic events are mediated by the prolongation of AP depolarization (Mitterdorfer and Bean, 2002) induced by the potassium channel blocker 4AP that facilitate IN-to-IN synaptic interactions. We also show that synaptic and direct electric coupling between IN could facilitate IN network hyperactivity that promotes SLE outburst.

At seizure onset, IN AP firing was enhanced. Even though all IN fire in coincidence with SLE onset, IN_{SOM} were activated first ahead of the SLE initiation as identified in field potential recordings. It should be mentioned that the exact identification of the extracellular seizure onset is not trivial. Still, the two methods we utilized to correlate both intracellular activities with the extracellular population discharge resulted in a clear divergent trend between IN and PYR, and suggest that PYR activate after IN and after the extracellular SLE initiation. Similar conclusions were reached during studies performed in EC mouse slices (Cammarota et al., 2013; Librizzi et al., 2017) that demonstrated a consistent precession of IN activity during 4AP-induced SLEs with simultaneous double recordings from pairs of IN and PYR.

LVF seizure onset could be induced by optogenetic activation of IN_{PV} or IN_{SOM} in the 4AP hippocampal and neocortical slice model (Dzhala and Staley, 2003; Shiri et al., 2015; Yekhlef et al., 2015; Chang et al., 2018) and in naïve and pilocarpine treated mice that express channelrhodopsin in IN_{PV} or IN_{SOM} (Shiri et al., 2015, 2016; Assaf and Schiller, 2016; Miri et al., 2018). On the other hand, optogenetic inhibition of PYR has been shown to reduce or prevent seizures in many seizure models (Chiang et al., 2014). A recent study reported that different IN subtypes control SLEs in somatosensory mouse cortex slices (Lado et al., 2022); in the presence of 4AP, light activation of channelrhodopsin-expressing IN_{PV} and IN_{SOM} (but not IN_{VIP}) evoked epileptiform discharges, suggesting that IN contribute differently to the initiation and inhibition of epileptiform discharges in cortical networks.

We confirmed the presence of DB in a subgroup of IN during both LVF and HYP SLEs (Cammarota et al., 2013). It is interesting to note that DB showed a clear trend to be much longer (3-4 sec) in IN in comparison to PYR (<1 sec). The possibility that the reduction in IN firing during DB could be responsible for the transition from a "preictal" condition of IN hyperactivity into the SLEs has been proposed in the past in the hight K^+ and the 4AP SLE models (Ziburkus et al., 2006; Cammarota et al., 2013). The permissive action of interneuronal DB to start seizures is not supported by our observation that only about 50% of IN undergo DB and also PYR display DB. In addition, SLE as extracellular population phenomenon initiates before DB develops. Based on previous experimental findings, we propose that DB is a cellular phenomenon associated to the abrupt neuronal depolarization beyond AP regeneration, possibly mediated by the fast changes in extracellular potassium generated by IN activity at seizure onset (Gnatkovsky et al., 2008; Trombin et al., 2011). Not surprisingly, we demonstrated that the presence of DB in individual IN depends on membrane potential depolarization level reached during SLE onset: when membrane potential returns to values suitable with reactivation of AP firing, SLEs progress into a phase of irregular AP firing that is followed within sec by the buildup of bursting activity that characterizes the final phase of a seizure (Devinsky et al., 2018).

Finally, we confirmed an important finding that has been reported by several *in vitro* studies, but seldom highlighted and discussed: all recorded IN generated robust firing throughout the late SLE phases. About one third of IN_{PV} and IN_{SOM} continuously fire high frequency APs from the onset of SLEs to its end, without evidence of DB. The large majority of IN discharged robust burst firing in synchrony with the local field

potential bursting discharges observed with extracellular electrodes. IN bursts during late SLEs are longer than field bursts in >90% IN_{CCK}, in >50% IN_{PV} and in >40% IN_{SOM} and was observed in about 30% PYR; the excessive firing during long IN bursts, together with high frequency firing observed in one third of IN_{PV} and IN_{SOM}, could be responsible for the inter-burst depression observed in this late SLE phase and could contribute to SLE termination.

An alternative mechanism that links neuronal hyperactivity to seizure termination was recently proposed; the massive bursting of IN networks together and in synchrony with PYR may produce a brief and transient condition of neuronal hyperactivity, followed by a synchronous post-burst depression mediated by both synaptic and extra synaptic events. When highly synchronous post-burst depression ensues, the synchrony of the next burst is enhanced, and the duration of the next post-burst depression progressively increases. As synchrony increases, inter-burst interval gets progressively longer to a critical point when the reactivation of a further burst is hampered: this mechanism leads seizures to stop (Boido et al., 2014b; Uva et al., 2021).

Conclusions

In the *in vitro* 4AP model of temporal lobe seizures, PV, CCK and SOM IN are very active at SLE onset, with IN_{SOM} consistently heralding the local field potential SLE initiation. IN are very active throughout all SLE phases and only about 50% show DB, this finding suggests that GABAergic IN run down is not required to boost seizure initiation and progression. Finally, IN hyperactivity in synchrony with PYR may contribute to seizure termination. The acute 4AP model generates SLEs that mimic seizure patterns commonly observed in human focal epilepsy and reproduces neuronal activities observed in patients during presurgical intracerebral monitoring. Based on this evidence, the 4AP model represents an excellent model to generate working hypotheses for future validation studies to be performed in different *in vivo* models and in humans.

456

457

458 **References**

459 Aracri P, Colombo E, Mantegazza M, Scalmani P, Curia G, Avanzini G, Franceschetti S (2006) Layer-
460 specific properties of the persistent sodium current in sensorimotor cortex. J Neurophysiol 95:3460–
461 3468.

462 Armstrong C, Wang J, Yeun Lee S, Broderick J, Bezaire MJ, Lee SH, Soltesz I (2016) Target-selectivity of
463 parvalbumin-positive interneurons in layer II of medial entorhinal cortex in normal and epileptic
464 animals. Hippocampus 26:779–793.

465 Assaf F, Schiller Y (2016) The antiepileptic and ictogenic effects of optogenetic neurostimulation of PV-
466 expressing interneurons. J Neurophysiol 116:1694–1704 Available at:
467 https://pubmed.ncbi.nlm.nih.gov/27486107/ [Accessed June 16, 2022].

468 Avoli M, Barbarosle M, Lücke A, Nagao T, Lopantsev V, Köhling R (1996a) Synchronous GABA-mediated
469 potentials and epileptiform discharges in the rat limbic system in vitro. J Neurosci 16:3912–3924.

470 Avoli M, de Curtis M (2011) GABAergic synchronization in the limbic system and its role in the generation
471 of epileptiform activity. Prog Neurobiol 95:104–132.

472 Avoli M, de Curtis M, Gnatkovsky V, Gotman J, Köhling R, Lévesque M, Manseau F, Shiri Z, Williams S
473 (2016) Specific imbalance of excitatory/inhibitory signaling establishes seizure onset pattern in
474 temporal lobe epilepsy. J Neurophysiol 115:3229–3237.

475 Avoli M, Louvel J, Kurcewicz I, Pumain R, Barbarosie M (1996b) Extracellular free potassium and calcium
476 during synchronous activity induced by 4-aminopyridine in the juvenile rat hippocampus. J Physiol 493
477 (Pt 3:707–717.

478 Avoli M, Psarropoulou C, Tancredi V, Fueta Y (1993) On the synchronous activity induced by 4-
479 aminopyridine in the CA3 subfield of juvenile rat hippocampus. J Neurophysiol 70:1018–1029.

480 Bean BP (2007) The action potential in mammalian central neurons. Nat Rev Neurosci 8:451–465.

481 Beed P, Gundlfinger A, Schneiderbauer S, Song J, Böhm C, Burgalossi A, Brecht M, Vida I, Schmitz D
482 (2013) Inhibitory gradient along the dorsoventral axis in the medial entorhinal cortex. Neuron 79:1197–
483 1207.

484 Behr C, D'Antuono M, Hamidi S, Herrington R, Lévesque M, Salami P, Shiri Z, Köhling R, Avoli M (2014)
485 Limbic networks and epileptiform synchronization: the view from the experimental side. Int Rev
486 Neurobiol 114:63–87.

487 Boido D, Gnatkovsky V, Uva L, Francione S, de Curtis M (2014a) Simultaneous enhancement of excitation
488 and postburst inhibition at the end of focal seizures. Ann Neurol 76:826–836.

Boido D, Jesuthasan N, de Curtis M, Uva L (2014b) Network dynamics during the progression of seizure-like events in the hippocampal-parahippocampal regions. Cereb Cortex 24:163–173.

Bragin A, Engel J, Wilson CL, Vizentin E, Mathern GW (1999) Electrophysiologic analysis of a chronic seizure model after unilateral hippocampal KA injection. Epilepsia 40:1210–1221.

Cammarota M, Losi G, Chiavegato A, Zonta M, Carmignoto G (2013) Fast spiking interneuron control of seizure propagation in a cortical slice model of focal epilepsy. J Physiol 591:807–822.

Cardin JA, Carlén M, Meletis K, Knoblich U, Zhang F, Deisseroth K, Tsai LH, Moore CI (2009) Driving fast-spiking cells induces gamma rhythm and controls sensory responses. Nature 459:663–667.

Chang M, Dian JA, Dufour S, Wang L, Moradi Chameh H, Ramani M, Zhang L, Carlen PL, Womelsdorf T, Valiante TA (2018) Brief activation of GABAergic interneurons initiates the transition to ictal events through post-inhibitory rebound excitation. Neurobiol Dis 109:102–116 Available at: https://pubmed.ncbi.nlm.nih.gov/29024712/.

Chever O, Zerimech S, Scalmani P, Lemaire L, Pizzamiglio L, Loucif A, Ayrault M, Krupa M, Desroches M, Duprat F, Léna I, Cestèle S, Mantegazza M (2021) Initiation of migraine-related cortical spreading depolarization by hyperactivity of GABAergic neurons and NaV1.1 channels. J Clin Invest 131.

Chiang CC, Ladas TP, Gonzalez-Reyes LE, Durand DM (2014) Seizure suppression by high frequency optogenetic stimulation using in vitro and in vivo animal models of epilepsy. Brain Stimul 7:890–899.

Codadu NK, Graham RT, Burman RJ, Jackson-Taylor RT, Raimondo J V., Trevelyan AJ, Parrish RR (2019) Divergent paths to seizure-like events. Physiol Rep 7.

Couey JJ, Witoelar A, Zhang SJ, Zheng K, Ye J, Dunn B, Czajkowski R, Moser MB, Moser EI, Roudi Y, Witter MP (2013) Recurrent inhibitory circuitry as a mechanism for grid formation. Nat Neurosci 16:318–324.

de Curtis M, Avoli M (2016) GABAergic networks jump-start focal seizures. Epilepsia 57:679–687.

Derchansky M, Jahromi SS, Mamani M, Shin DS, Sik A, Carlen PL (2008) Transition to seizures in the isolated immature mouse hippocampus: a switch from dominant phasic inhibition to dominant phasic excitation. J Physiol 586:477–494.

Devinsky O, Vezzani A, O'Brien TJ, Jette N, Scheffer IE, de Curtis M, Perucca P (2018b) Epilepsy. Nat Rev Dis Prim 4.

Di Cristo G, Awad PN, Hamidi S, Avoli M (2018) KCC2, epileptiform synchronization, and epileptic disorders. Prog Neurobiol 162:1–16.

Di Giacomo R, Uribe-San-Martin R, Mai R, Francione S, Nobili L, Sartori I, Gozzo F, Pelliccia V, Onofrj

M, Lo Russo G, de Curtis M, Tassi L (2019) Stereo-EEG ictal/interictal patterns and underlying pathologies. Seizure 72:54–60.

Dzhala VI, Staley KJ (2003) Excitatory actions of endogenously released GABA contribute to initiation of ictal epileptiform activity in the developing hippocampus. J Neurosci 23:1840–1846.

Elahian B, Lado NE, Mankin E, Vangala S, Misra A, Moxon K, Fried I, Sharan A, Yeasin M, Staba R, Bragin A, Avoli M, Sperling MR, Engel J, Weiss SA (2018) Low-voltage fast seizures in humans begin with increased interneuron firing. Ann Neurol 84:588–600.

Engel J (1990) The Hans Berger lecture. Functional explorations of the human epileptic brain and their therapeutic implications. Electroencephalogr Clin Neurophysiol 76:296–316.

Fernandez FR, Via G, Canavier CC, White JA (2022) Kinetics and Connectivity Properties of Parvalbumin- and Somatostatin-Positive Inhibition in Layer 2/3 Medial Entorhinal Cortex. eNeuro 9.

Ferrante M, Tahvildari B, Duque A, Hadzipasic M, Salkoff D, Zagha EW, Hasselmo ME, McCormick DA (2017) Distinct Functional Groups Emerge from the IntrINic Properties of Molecularly Identified Entorhinal Interneurons and Principal Cells. Cereb Cortex 27:3186–3207.

Freund TF, Buzsáki G (1996) Interneurons of the hippocampus. Hippocampus 6:347–470.

Fuchs EC, Neitz A, Pinna R, Melzer S, Caputi A, Monyer H (2016) Local and Distant Input Controlling Excitation in Layer II of the Medial Entorhinal Cortex. Neuron 89:194–208.

Fujita S, Toyoda I, Thamattoor AK, Buckmaster PS (2014) Preictal activity of subicular, CA1, and dentate gyrus principal neurons in the dorsal hippocampus before spontaneous seizures in a rat model of temporal lobe epilepsy. J Neurosci 34:16671–16687.

Fujiwara-Tsukamoto Y, Isomura Y, Imanishi M, Fukai T, Takada M (2007) Distinct types of ionic modulation of GABA actions in pyramidal cells and interneurons during electrical induction of hippocampal seizure-like network activity. Eur J Neurosci 25:2713–2725.

Gallopin T, Geoffroy H, Rossier J, Lambolez B (2006) Cortical sources of CRF, NKB, and CCK and their effects on pyramidal cells in the neocortex. Cereb Cortex 16:1440–1452.

Gnatkovsky V, Librizzi L, Trombin F, de Curtis M (2008) Fast activity at seizure onset is mediated by inhibitory circuits in the entorhinal cortex in vitro. Ann Neurol 64:674–686.

Gnatkovsky V, Pelliccia V, de Curtis M, Tassi L (2019) Two main focal seizure patterns revealed by intracerebral electroencephalographic biomarker analysis. Epilepsia 60:96–106.

Goff KM, Goldberg EM (2019) Vasoactive intestinal peptide-expressing interneurons are impaired in a mouse model of Dravet syndrome. Elife 8.

551 Goldberg EM, Clark BD, Zagha E, Nahmani M, Erisir A, Rudy B (2008) K+ channels at the axon initial
552 segment dampen near-threshold excitability of neocortical fast-spiking GABAergic interneurons.
553 Neuron 58:387–400.

554 Grasse DW, Karunakaran S, Moxon KA (2013) Neuronal synchrony and the transition to spontaneous
555 seizures. Exp Neurol 248:72–84.

556 Helm J, Akgul G, Wollmuth LP (2013) Subgroups of parvalbumin-expressing interneurons in layers 2/3 of
557 the visual cortex. J Neurophysiol 109:1600–1613.

558 Hjorth J, Blackwell KT, Kotaleski JH (2009) Gap junctions between striatal fast-spiking interneurons
559 regulate spiking activity and synchronization as a function of cortical activity. J Neurosci 29:5276–
560 5286.

561 Jenerick H (1963) PHASE PLANE TRAJECTORIES OF THE MUSCLE SPIKE POTENTIAL. Biophys J
562 3:363–377.

563 Kaila K, Lamsa K, Smirnov S, Taira T, Voipio J (1997) Long-lasting GABA-mediated depolarization
564 evoked by high-frequency stimulation in pyramidal neurons of rat hippocampal slice is attributable to a
565 network-driven, bicarbonate-dependent K+ transient. J Neurosci 17:7662–7672.

566 Kaila K, Ruusuvuori E, Seja P, Voipio J, Puskarjov M (2014) GABA actions and ionic plasticity in epilepsy.
567 Curr Opin Neurobiol 26:34–41.

568 Karson MA, Tang AH, Milner TA, Alger BE (2009) Synaptic cross talk between perisomatic-targeting
569 interneuron classes expressing cholecystokinin and parvalbumin in hippocampus. J Neurosci 29:4140–
570 4154.

571 Kawaguchi Y, Kondo S (2002) Parvalbumin, somatostatin and cholecystokinin as chemical markers for
572 specific GABAergic interneuron types in the rat frontal cortex. J Neurocytol 31:277–287.

573 Kecskés M, Henn-Mike N, Agócs-Laboda Á, Szőcs S, Petykó Z, Varga C (2020) Somatostatin expressing
574 GABAergic interneurons in the medial entorhinal cortex preferentially inhibit layer III-V pyramidal
575 cells. Commun Biol 3.

576 Klausberger T, Marton LF, O'Neill J, Huck JHJ, Dalezios Y, Fuentealba P, Suen WY, Papp E, Kaneko T,
577 Watanabe M, Csicsvari J, Somogyi P (2005) Complementary roles of cholecystokinin- and
578 parvalbumin-expressing GABAergic neurons in hippocampal network oscillations. J Neurosci
579 25:9782–9793.

580 Köhling R, D'Antuono M, Benini R, de Guzman P, Avoli M (2016) Hypersynchronous ictal onset in the
581 perirhinal cortex results from dynamic weakening in inhibition. Neurobiol Dis 87:1–10.

582 Lado WE, Xu X, Hablitz JJ (2022) Modulation of epileptiform activity by three subgroups of GABAergic
583 interneurons in mouse somatosensory cortex. Epilepsy Res 183.

584 Lagarde S, Bonini F, McGonigal A, Chauvel P, Gavaret M, Scavarda D, Carron R, Régis J, Aubert S,
585 Villeneuve N, Giusiano B, Figarella-Branger D, Trebuchon A, Bartolomei F (2016) Seizure-onset
586 patterns in focal cortical dysplasia and neurodevelopmental tumors: Relationship with surgical
587 prognosis and neuropathologic subtypes. Epilepsia 57:1426–1435.

588 Lasztóczi B, Nyitrai G, Héja L, Kardos J (2009) Synchronization of GABAergic inputs to CA3 pyramidal
589 cells precedes seizure-like event onset in juvenile rat hippocampal slices. J Neurophysiol 102:2538–
590 2553.

591 Lemaire L, Desroches M, Krupa M, Pizzamiglio L, Scalmani P, Mantegazza M (2021) Modeling
592 NaV1.1/SCN1A sodium channel mutations in a microcircuit with realistic ion concentration dynamics
593 suggests differential GABAergic mechanisms leading to hyperexcitability in epilepsy and hemiplegic
594 migraine. PLoS Comput Biol 17.

595 Lévesque M, Chen LY, Hamidi S, Avoli M (2018) Dynamic interneuron-principal cell interplay leads to a
596 specific pattern of in vitro ictogenesis. Neurobiol Dis 115:92–100.

597 Lévesque M, Salami P, Behr C, Avoli M (2013) Temporal lobe epileptiform activity following systemic
598 administration of 4-aminopyridine in rats. Epilepsia 54:596–604.

599 Librizzi L, Losi G, Marcon I, Sessolo M, Scalmani P, Carmignoto G, de Curtis M (2017) Interneuronal
600 Network Activity at the Onset of Seizure-Like Events in Entorhinal Cortex Slices. J Neurosci
601 37:10398–10407.

602 Lopantsev V, Avoli M (1998a) Participation of GABAA-mediated inhibition in ictallike discharges in the rat
603 entorhinal cortex. J Neurophysiol 79:352–360.

604 Lopantsev V, Avoli M (1998b) Laminar organization of epileptiform discharges in the rat entorhinal cortex
605 in vitro. J Physiol 509 (Pt 3:785–796.

606 López-Bendito G, Sturgess K, Erdélyi F, Szabó G, Molnár Z, Paulsen O (2004) Preferential origin and layer
607 destination of GAD65-GFP cortical interneurons. Cereb Cortex 14:1122–1133.

608 Losi G, Cammarota M, Chiavegato A, Gomez-Gonzalo M, Carmignoto G (2010) A new experimental model
609 of focal seizures in the entorhinal cortex. Epilepsia 51:1493–1502.

610 Mantegazza M, Franceschetti S, Avanzini G (1998) Anemone toxin (ATX II)-induced increase in persistent
611 sodium current: effects on the firing properties of rat neocortical pyramidal neurones. J Physiol 507 (Pt
612 1:105–116.

613 Merricks EM, Smith EH, Emerson RG, Bateman LM, McKhann GM, Goodman RR, Sheth SA, Greger B,
614 House PA, Trevelyan AJ, Schevon CA (2021) Neuronal Firing and Waveform Alterations through Ictal
615 Recruitment in Humans. J Neurosci 41:766–779.

616 Miri ML, Vinck M, Pant R, Cardin JA (2018) Altered hippocampal interneuron activity precedes ictal onset.
617 Elife 7.

618 Mitterdorfer J and Bean BP (2002) Potassium Currents during the Action Potential of Hippocampal CA3
619 Neurons. J Neurosci, 22:10106–10115.

620 Miyamae T, Chen K, Lewis DA, Gonzalez-Burgos G (2017) Distinct Physiological Maturation of
621 Parvalbumin-Positive Neuron Subtypes in Mouse Prefrontal Cortex. J Neurosci 37:4883–4902.

622 Neske GT, Patrick SL, Connors BW (2015) Contributions of diverse excitatory and inhibitory neurons to
623 recurrent network activity in cerebral cortex. J Neurosci 35:1089–1105.

624 Nguyen R, Venkatesan S, Binko M, Bang JY, Cajanding JD, Briggs C, Sargin D, Imayoshi I, Lambe EK,
625 Kim JC (2020) Cholecystokinin-Expressing Interneurons of the Medial Prefrontal Cortex Mediate
626 Working Memory Retrieval. J Neurosci 40:2314–2331.

627 Pelkey KA, Chittajallu R, Craig MT, Tricoire L, Wester JC, McBain CJ (2017) Hippocampal GABAergic
628 Inhibitory Interneurons. Physiol Rev 97:1619–1747.

629 Perez Velazquez JL, Carlen PL (1999) Synchronization of GABAergic interneuronal networks during
630 seizure-like activity in the rat horizontal hippocampal slice. Eur J Neurosci 11:4110–4118.

631 Perucca P, O'Brien TJ (2015) Epilepsy in 2014. Novel and large collaborations drive advances in epilepsy.
632 Nat Rev Neurol 11:74–76.

633 Pfeffer CK, Xue M, He M, Huang ZJ, Scanziani M (2013) Inhibition of inhibition in visual cortex: the logic
634 of connections between molecularly distinct interneurons. Nat Neurosci 16:1068–1076.

635 Riban V, Bouilleret V, Pham-Lê BT, Fritschy JM, Marescaux C, Depaulis A (2002) Evolution of
636 hippocampal epileptic activity during the development of hippocampal sclerosis in a mouse model of
637 temporal lobe epilepsy. Neuroscience 112:101–111.

638 Rudy B, Fishell G, Lee SH, Hjerling-Leffler J (2011) Three groups of interneurons account for nearly 100%
639 of neocortical GABAergic neurons. Dev Neurobiol 71:45–61.

640 Shiri Z, Manseau F, Lévesque M, Williams S, Avoli M (2015) Interneuron activity leads to initiation of low-
641 voltage fast-onset seizures. Ann Neurol 77:541–546.

642 Shiri Z, Manseau F, Lévesque M, Williams S, Avoli M (2016) Activation of specific neuronal networks
643 leads to different seizure onset types. Ann Neurol 79:354–365.

644 Singh S, Sandy S, Wiebe S (2015) Ictal onset on intracranial EEG: Do we know it when we see it? State of
645 the evidence. Epilepsia 56:1629–1638.

646 Tamamaki N, Yanagawa Y, Tomioka R, Miyazaki JI, Obata K, Kaneko T (2003) Green fluorescent protein
647 expression and colocalization with calretinin, parvalbumin, and somatostatin in the GAD67-GFP
648 knock-in mouse. J Comp Neurol 467:60–79.

649 Toyoda I, Fujita S, Thamattoor AK, Buckmaster PS (2015) Unit Activity of Hippocampal Interneurons
650 before Spontaneous Seizures in an Animal Model of Temporal Lobe Epilepsy. J Neurosci 35:6600–
651 6618.

652 Tremblay R, Lee S, Rudy B (2016) GABAergic Interneurons in the Neocortex: From Cellular Properties to
653 Circuits. Neuron 91:260–292.

654 Tricoire L, Pelkey KA, Erkkila BE, Jeffries BW, Yuan X, McBain CJ (2011) A blueprint for the
655 spatiotemporal origIN of mouse hippocampal interneuron diversity. J Neurosci 31:10948–10970.

656 Trombin F, Gnatkovsky V, de Curtis M (2011) Changes in action potential features during focal seizure
657 discharges in the entorhinal cortex of the in vitro isolated guinea pig brain. J Neurophysiol 106:1411–
658 1423.

659 Truccolo W, Donoghue JA, Hochberg LR, Eskandar EN, Madsen JR, Anderson WS, Brown EN, Halgren E,
660 Cash SS (2011) Single-neuron dynamics in human focal epilepsy. Nat Neurosci 14:635–643.

661 Urban-Ciecko J, Barth AL (2016) Somatostatin-expressing neurons in cortical networks. Nat Rev Neurosci
662 17:401–409.

663 Uva L, Aracri P, Forcaia G, de Curtis M (2021) Mapping region-specific seizure-like patterns in the in vitro
664 isolated guinea pig brain. Exp Neurol 342.

665 Uva L, Avoli M, de Curtis M (2009) Synchronous GABA-receptor-dependent potentials in limbic areas of
666 the in-vitro isolated adult guinea pig brain. Eur J Neurosci 29:911–920.

667 Uva L, Boido D, Avoli M, de Curtis M, Lévesque M (2017a) High-frequency oscillations and seizure-like
668 discharges in the entorhinal cortex of the in vitro isolated guinea pig brain. Epilepsy Res 130:21–26.

669 Uva L, Breschi GL, Gnatkovsky V, Taverna S, de Curtis M (2015) Synchronous inhibitory potentials
670 precede seizure-like events in acute models of focal limbic seizures. J Neurosci 35:3048–3055.

671 Uva L, Librizzi L, Wendling F, De Curtis M (2005) Propagation dynamics of epileptiform activity acutely
672 induced by bicuculline in the hippocampal-parahippocampal region of the isolated Guinea pig brain.
673 Epilepsia 46:1914–1925.

674 Uva L, Saccucci S, Chikhladze M, Tassi L, Gnatkovsky V, Milesi G, Morbin M, de Curtis M (2017b) A

675 Novel Focal Seizure Pattern Generated in Superficial Layers of the Olfactory Cortex. J Neurosci
676 37:3544–3554.

677 Uva L, Trombin F, Carriero G, Avoli M, de Curtis M (2013) Seizure-like discharges induced by 4-
678 aminopyridine in the olfactory system of the in vitro isolated guinea pig brain. Epilepsia 54:605–615.

679 Varga C, Lee SY, Soltesz I (2010) Target-selective GABAergic control of entorhinal cortex output. Nat
680 Neurosci 13:822–824.

681 Weiss SA, Staba R, Bragin A, Moxon K, Sperling M, Avoli M, Engel J (2019) "Interneurons and principal
682 cell firing in human limbic areas at focal seizure onset." Neurobiol Dis 124:183–188.

683 Yekhlef L, Breschi GL, Lagostena L, Russo G, Taverna S (2015) Selective activation of parvalbumin- or
684 somatostatin-expressing interneurons triggers epileptic seizurelike activity in mouse medial entorhinal
685 cortex. J Neurophysiol 113:1616–1630.

686 Zhang ZJ, Koifman J, Shin DS, Ye H, Florez CM, Zhang L, Valiante TA, Carlen PL (2012) Transition to
687 seizure: ictal discharge is preceded by exhausted presynaptic GABA release in the hippocampal CA3
688 region. J Neurosci 32:2499–2512.

689 Ziburkus J, Cressman JR, Barreto E, Schiff SJ (2006) Interneuron and pyramidal cell interplay during in
690 vitro seizure-like events. J Neurophysiol 95:3948–3954.

691

692

693 **Figures**

694 **Fig. 1. Different types of interneurons identified by firing properties:** IN recorded in EC slices with
695 typical features of IN_{PV} (red traces/plots), IN_{CCK} (green), IN_{SOM} (blue) and typical pyramidal neuron (PYR,
696 black) are illustrated; different firing properties were observed in IN_{SOM} recorded either in superficial (2/3) of
697 deep (4/5) EC layers (light blue and dark blue, respectively). **A:** Representative traces of action potential
698 (AP) firing recorded from IN and PYR in GAD-67/65 mouse EC slices, elicited by intracellular injection of a
699 2.5 s depolarizing pulse (bottom row); the 3 traces illustrate responses evoked by current pulses just below
700 (bottom traces) and just above AP threshold (middle trace), and by large current pulses (upper rows).
701 Asterisks mark post-AP afterhyperpolarizing potentials (AHP) in IN_{PV} and $IN_{SOM4/5}$; the arrowhead points to
702 the delayed AP firing at threshold depolarization typically observed in IN_{PV}; arrows mark AP bursting at
703 threshold typical of IN_{CCK} (see results). **B:** Average firing rates of IN and PYR constructed from I/O plots
704 that display the AP frequency in response to intracellular depolarizing current pulses of increasing amplitude.
705 The curves describe the average data (mean ± SD) obtained from 17 IN_{PV}, 11 IN_{CCK}, 6 $IN_{SOM2/3,}$ 9 $IN_{SOM\ 4/5}$
706 and 10 PYR neurons. **C:** Average AP phase plots showing the first derivative of membrane potential changes
707 as a function of instantaneous AP membrane potential (dV/dt *vs* mV) for the different types of IN and PYR
708 (see also Fig. 1-2A-B). APs are represented as a loop in which the starting point is the threshold membrane
709 potential, and the extreme right point is the maximal AP voltage amplitude. Each panel represents the
710 average of 16 IN_{PV}, 11 IN_{CCK}, 5 $IN_{SOM2/3}$, 9 $IN_{SOM4/5}$ and 10 PYR. The arrowheads in the left panel and in the
711 sec panel from the right indicate the two AP accelerations typically observed in IN_{PV} and $IN_{SOM4/5}$. **D:**
712 Average inter-spike intervals of the first 11 APs evoked by intracellular depolarizing current injection just
713 above firing threshold, in IN_{PV} (red; n=16), IN_{CCK} (green, n=12), $IN_{SOM2/3}$ (light blue; n=5), $IN_{SOM4/5}$ (blue,
714 n=8) and PYR (black; n=10) neurons. **E:** Percentage of adapting (black column) and non-adapting (striped
715 column) neurons divided per IN subtypes and PYR. Adapting neurons; IN_{PV}=0%, IN_{CCK}=92.3%,
716 $IN_{SOM2/3}$=66.6%, $IN_{SOM4/5}$=11.1% and PYR=100%. Non Adapting neurons; IN_{PV}=100%, IN_{CCK}=7.7%,
717 $IN_{SOM2/3}$=33.4%, $IN_{SOM4/5}$=88.9% and PYR=0%. For statistical analysis, Fisher Exact test with Bonferroni's
718 correction was used (*=P<0.05, **=P<0.01, ***=P<<<0.01).

719 **Fig. 2. Single-cell digital PCR analysis of IN subgroups. A-C:** Expression of *Pv* (red), *Cck* (green), and
720 *Som* (blue) cDNA in 11, 12 and 12 IN, respectively, defined as IN_{PV} (**A**), IN_{CCK} (**B**) and IN_{SOM} (**C**) based on
721 electrophysiological properties. The result, expressed as copies/µl, were normalized assuming that the total
722 copies/µl of all targets (PV+CCK+SOM) is equal to 100 (%); the percentage of each target was calculated as
723 relative ratio. For statistical analysis and data distribution ANOVA with Tukey's multiple comparison test
724 was used; for data not normally distributed Kruskal Wallis test with Dunn's multiple comparison test was
725 utilized (*=P<0.05, **=P<0.01, ***=P<<<0.01).

726 **Fig. 3. Firing patterns of interneurons and pyramidal cells during SLEs induced by slice perfusion**
727 **with 100 µM 4AP in 0.5 mM Mg^{2+}. A: SLE characterized by a low-voltage fast activity onset (LVF;**
728 **arrow) recorded with an extracellular electrode (lower trace) and simultaneously recorded from an**
729 **IN_{PV} with a patch electrode (upper trace). B: LVF-onset SLE (arrow) simultaneously recorded from a**
730 **PYR neuron (upper trace) and with an extracellular electrode (lower trace). Note that IN discharge**
731 **from the very onset of SLEs (A), whereas the PYR is activated after SLE onset (B). C: SLE**
732 **characterized by a hypersynchronous activity pattern (HYP; arrows on large spikes in the lower trace)**
733 **intracellularly recorded from an IN_{SOM} (upper trace). Arrowheads point to synaptic background**
734 **activity generated during 4AP perfusion – see also D. D: Simultaneous extracellular (lower traces) and**
735 **intracellular (upper tracers) recordings during the pre-ictal activity observed in an INPV (a) and an**
736 **INCCK (b); spontaneous synaptic activity was observed in correlation with extracellular pre-ictal**
737 **spikes. E: Upper plot, quantification of AP numbers during 3-minute perfusion with control ACSF**
738 **before 4AP application in INPV (237 ± 58.66, n=15, red dots), INCCK (124.20 ± 32.49, n=11, green**
739 **dots), INSOM2/3 (1.6 ± 1.6, n=5, cyan dots), INSOM4/5 (6.87 ± 4.37, n=8, blue dots) and in PYR (2.5 ±**
740 **1.43925, N=9, black dots). Lower plot, quantification of AP numbers during in 4AP, 3 minutes before**
741 **the onset of SLEs: INPV (237 ± 58.66, n=15, red dots), INCCK (124.20 ± 32.49, n=11, green dots),**
742 **INSOM2/3 (421.4 ± 184.3, n=5, cyan dots), INSOM4/5 (380.37 ± 129.38, n=8, blue dots) and in PYR**
743 **(2.5 ± 1.43925, N=9, black dots). Kruskal Wallis test with Dunn's multiple comparison test (*=P<0.05,**
744 ****=P<0.01, ***=P<<<0.01).**

745 **Fig. 4. $GABA_A$ receptor dependence of epileptiform events induced by 4AP. A.** Representative
746 experiment performed with field potential extracellular recordings during 4AP (light grey bar), co-perfused
747 with kynurenic acid (KYN; dark grey bar) and co-perfused with **kynurenic acid** and picrotoxin (PTX; black
748 bar). A SLE is generated during long reperfusion with 4AP. The pre-ictal epileptiform spikes were not
749 altered by KYN and were abolished by PTX. **B. Representative experiment performed with field**
750 **potential extracellular recordings during 4AP (light grey bar) co-perfused with PTX (black bar) and**
751 **at the end perfused only with 4AP which induced SLE. During 4AP + PTX co-perfusion only**
752 **population spikes (but not SLE) were activated, whereas perfusion of 4AP promoted a SLE and an**
753 **increase of background activity.**

754 **Fig. 5: Correlation between extracellular SLE onset and the activity of IN and PYR. A: Two**
755 **parameters were utilized to measure the delay between the neuronal and extracellular SLE onset. In**
756 **the upper panel the activity simultaneously recorded with an extracellular electrode (lower trace) and**
757 **from an IN (IN_{SOM}) with a patch electrode (upper trace). In the lower panel the traces in the dashed**
758 **square of the upper panel are shown with an expanded time scale. The arrows indicate the first action**
759 **potential peak; the arrowhead point to the onset of depolarization; the right dashed line marks SLE**
760 **onset in the extracellular trace. Delay measurements *a* and *b* are illustrated for all neurons in graphs**
761 **Ba and Bb respectively. Ba: The delay between the peak of the first ictal AP recorded in neurons**
762 **(arrow) and the onset of the extracellular fast activity at SLE onset (time 0) was considered; for HYP**
763 **SLEs, time 0 was the first extracellular spike burst (not shown). Using these parameters, IN_{pv} (-204.92**
764 **± 332.16 ms, n=16, red dots), IN_{CCK} (-3135.93 ± 2099.16 ms, n=9, green dots) and $IN_{SOM2/3}$ (-125.6 ± 61.8**
765 **ms, n=5, cyan dots) and $IN_{SOM4/5}$ (-800.13 ± 556.79 ms, n=8, blue dots); PYR showed a higher**
766 **variability and started to fire after SLE onset (+5824.1 ± 2388.25 ms, n=10, black dots). AP firing**
767 **showed statistical significance when IN_{CCK} were compared with PYR (asterisk on the right). Bb: Plot**
768 **of the delay between the first pre-ictal intracellular depolarizing potential (arrowhead) recorded and**
769 **the onset of the slow deflection associated with extracellular SLE onset (time 0): IN_{PV} (-32.82 ± 22.55**
770 **ms, n=13), IN_{CCK} (-42.71 ± 18.37 ms, n=8) and $IN_{SOM2/3}$ (-103.75 ± 24.12 mse, n=4) and $IN_{SOM4/5}$ (117.6 ±**
771 **51.74 sec, n=5) activated before or around the onset of the extracellular SLE.. Statistically significant**
772 **delays between IN subgroups are illustrated by asterisks on the right of box charts. PYR were active in**

coincidence or after SLE slow deflection (+3579.08 ± 1464.22 sec; n=8). IN_{SOM} activity consistently started before PYR (asterisk on the right of box chart). C: Same graph shown in Bb is illustrated with extended time scale, without PYR data. Kruskal Wallis test with Dunn's multiple comparison test. (*=P<0.05, **=P<0.01, ***=P<<<0.01).

Fig. 6: Depolarizing block after SLEs induced by 4AP. A: Representative LVF SLE recorded with an extracellular electrode (lower trace) and with a patch electrode from an IN (upper trace); the arrowhead indicates the depolarizing block (DB) after SLE onset. **B: Percentage of cells that showed DB (IN_{PV}= 37.5%, IN_{CCK}= 50%, $IN_{SOM2/3}$= 60%, $IN_{SOM4/5}$= 80% and PYR= 40%, black columns) and did not show DB (IN_{PV}= 62.5%, IN_{CCK}= 50%, $IN_{SOM2/3}$= 40%, $IN_{SOM4/5}$= 20% and PYR= 60%, striped columns). C: Quantification of maximal membrane potential depolarization value measured in IN_{PV}, IN_{CCK} and IN_{SOM} during SLE: membrane potential values of IN that show (left columns) and did not show DB (right columns) are illustrated (*=P<0.05, ***=P<<<0.01). All INs with DB showed membrane depolarization above -30 mV. Statistical analysis could not be performed for $IN_{SOM2/3}$ and $IN_{SOM4/5}$ because of the small sample size. D: DB duration (in sec) in IN_{PV} (4.56 ± 1.36, n=6, red dots), IN_{CCK} (3.97 ± 2.20, n=5, green dots), $IN_{SOM2/3}$ (2.8 ± 1.62, n=3, cyan dots), $IN_{SOM4/5}$ (3.93 ± 1.12, n=7, blue dots) and PYR (0.95 ± 0.19, n=4, black dots). The data show no significant difference in the duration of the DB, ANOVA with Tukey's multiple comparison test were used.**

Fig. 7: Different firing patterns during the late phase at the end of SLEs. A: On the top, burst firing recorded with the whole-cell patch electrodes (upper traces) or the extracellular electrodes (lower traces) during the late phase of SLEs induced by 4AP perfusion. In the IN illustrated in **a**, the duration of the extra and intracellular bursts are similar. Intracellular burst firing lasted longer than the simultaneous extracellular burst discharge in the IN shown in **b**. High frequency firing not related with SLEs extracellular bursting activity was recorded from the IN in **c**. **B**: expanded traces of the 3 different late SLE patterns illustrated in **A**. **C: Percentage of neurons (IN_{pv}, IN_{CCK}, $IN_{SOM2/3}$, $IN_{SOM4/5}$, and PYR) showing the three patterns displayed in A. Short burst were recorded in 18.75% IN_{PV}, 8.33% IN_{CCK}, 0% $IN_{SOM2/3}$, 37.5% $IN_{SOM4/5}$, and 66.66% PYR (black columns); long-lasting intracellular bursts were observed in 43.75% IN_{PV}, 91.66 % IN_{CCK}, 80% $IN_{SOM2/3}$, 37.5% $IN_{SOM4/5}$, and 33.33% PYR (striped columns); high frequency**

firing not correlated with extracellular bursting was found in 37.5% IN_{PV}, 0% IN_{CCK}, 20% $IN_{SOM2/3}$, 25% $IN_{SOM4/5}$ and 0% PYR (empty columns). Chi-Square "Goodness of Fit" test showed that PYR displayed more short burst discharges than other types of firing (P = 0.049) and IN_{CCK} more long-lasting intracellular bursts than other types of firing (P = 0.0001); IN_{PV} and IN_{SOM} did not show a favorite type of firing.

Extended data Figure 1-1. Experimental set-up. A: Microphotograph of a horizontal hippocampal/entorhinal mouse slice (10x magnification). Local field potential (LFPe) and patch-clamp (PCe) recording electrodes are illustrated. EC: entorhinal cortex; hip: hippocampal formation. High magnification images have been obtained with infrared DIC (**B**) and fluorescence microscopy (**C**). GFP-containing IN (red arrow) in an EC slice from GAD65 and GAD67 mouse and GFP-negative neurons (black arrows) with typical pyramidal soma. **D:** Percentage of IN subtypes recoded in EC slices obtained from GAD65 (IN_{PV}= 14.3%, IN_{CCK}= 83.3%, IN_{SOM}= 0%, PYR= 0%, striped columns) and GAD67 mice (IN_{PV}= 85.7%, IN_{CCK}= 16.7%, IN_{SOM}= 100%, PYR= 0%, black columns). **E:** Percentage of IN subtypes and PYR recorded from superficial EC layers 2-3 (IN_{PV}= 70%, IN_{CCK}= 77%, IN_{SOM}= 40%, PYR= 80%, black columns) and deep EC layers 4 and 5 (IN_{PV}= 30%, IN_{CCK}= 23%, IN_{SOM}= 60%, PYR= 20%, striped columns). For statistical analysis, Fisher Exact test with Bonferroni's correction was used (*=P<0.05, **=P<0.01, ***=P<<<0.01).

Extended data Figure 1-2: **Main features of APs recorded from the different subtypes of IN and PYR. A:** Representative trace of AP (continuous line) and its first derivative (dashed line) utilized to construct AP phase plots. The y axis refer to the AP (right) and the first derivative (left) respectively, the pink dotted line indicates the alignment used to create the phase plots shown in B. **B:** AP phase plots of the different subtypes of EC neurons. The arrows indicate the parameters analyzed in Figures C-F. **C:** AP threshold quantification (in mV), IN_{PV}= -41.57 ± 0.80; IN_{CCK}= -47.54 ± 1.20; $IN_{SOM2/3}$= -44.50 ± 2.82; $IN_{SOM4/5}$= -45.73 ± 1.06; PYR= -46.73 ± 1.27 **D:** AP peak amplitude quantification (in mV), IN_{PV}= 29.93 ± 1.17; IN_{CCK}= 29.86 ± 2.21; $IN_{SOM2/3}$= 34.30 ± 4.36; $IN_{SOM4/5}$= 35.21 ± 2.23; PYR= 40.97 ± 2.83. **E:** Max rise slope quantification (mV/ms), IN_{PV}= 218.40 ± 10.26; IN_{CCK}= 233.97 ± 8.28; $IN_{SOM2/3}$= 237.88 ± 31.96;

827 $IN_{SOM4/5}$= 305.20 ± 23.82; PYR= 255.55 ± 22.76. **F:** Max decay slope quantification (mV/ms). IN_{PV}= -50.61
828 ± 1.75; IN_{CCK}= -65.37 ± 3.6; $IN_{SOM2/3}$= -77.33 ± 10.16; $IN_{SOM4/5}$= -132.56 ± 22.06; PYR= -50.09 ± 3.28. IN_{PV}
829 (red dots, n=16), IN_{CCK} (green dots, n=11), $IN_{SOM2/3}$ (light blue dots, n=5), $IN_{SOM4/5}$ (blue dots, n=9) and PYR
830 (black dots, n=10). ANOVA with Tukey's multiple comparison test and Kruskal Wallis test with Dunn's
831 multiple comparison test were used. (*=P<0.05, **=P<0.01, ***=P<<<0.01).

832 **Extended data Figure 2-1**: **Electrophysiological features of IN_{PV} with elevated CCK cDNA content**.
833 Data obtained in IN_{PV} that expressed CCK at levels higher than PV are illustrated by purple dots and lines
834 (n=4); red symbols mark data from the remaining IN_{PV} group (n=13); green symbols identify IN_{CCK} data
835 (n=13). **A:** Average firing rate (I/O plot) of IN in response to intracellular current pulses of increasing
836 amplitude: **B:** Average interval between the first 11 action potential (AP) evoked by intracellular
837 depolarizing current injection just over the threshold. **C:** Averaged AP phase plots showing the derivative of
838 membrane potential (dV/dt *vs* mV) as a function of Instantaneous membrane potential during action potential
839 for the different groups of IN. The data confirm that the 4 IN_{PV} with high CCK content showed
840 electrophysiological features different from IN_{CCK}.

841 **Table 1. Digital PCR Assay Details.** Fluorescein (FAM): is a fluorescent dye with an absorption wave
842 length of 495 nm and an emission wavelength of 517 nm modified Aequora Victoria fluorescein, 6-VIC is a
843 fluorescent compound with an excitation peak at 526 nm and an emission peak at 543 nm.

Gene symbol	Assay ID	Ref Seq:	Probe Exon Location	Amplicon Size	Probe Dye
Cck	Mm00446170_m1	NM_031161.4	Probe spans exons 2-3	79	FAM
Pv	Mm00443100_m1	NM_013645.3	Probe spans exons 1-2	77	FAM
Som	Mm00436671_m1	NM_009215.1	Probe spans exons 1-2	86	FAM
Gapdh	Mm99999915-g1	NM_008084.3	Probe spans exons 2-3	109	VIC

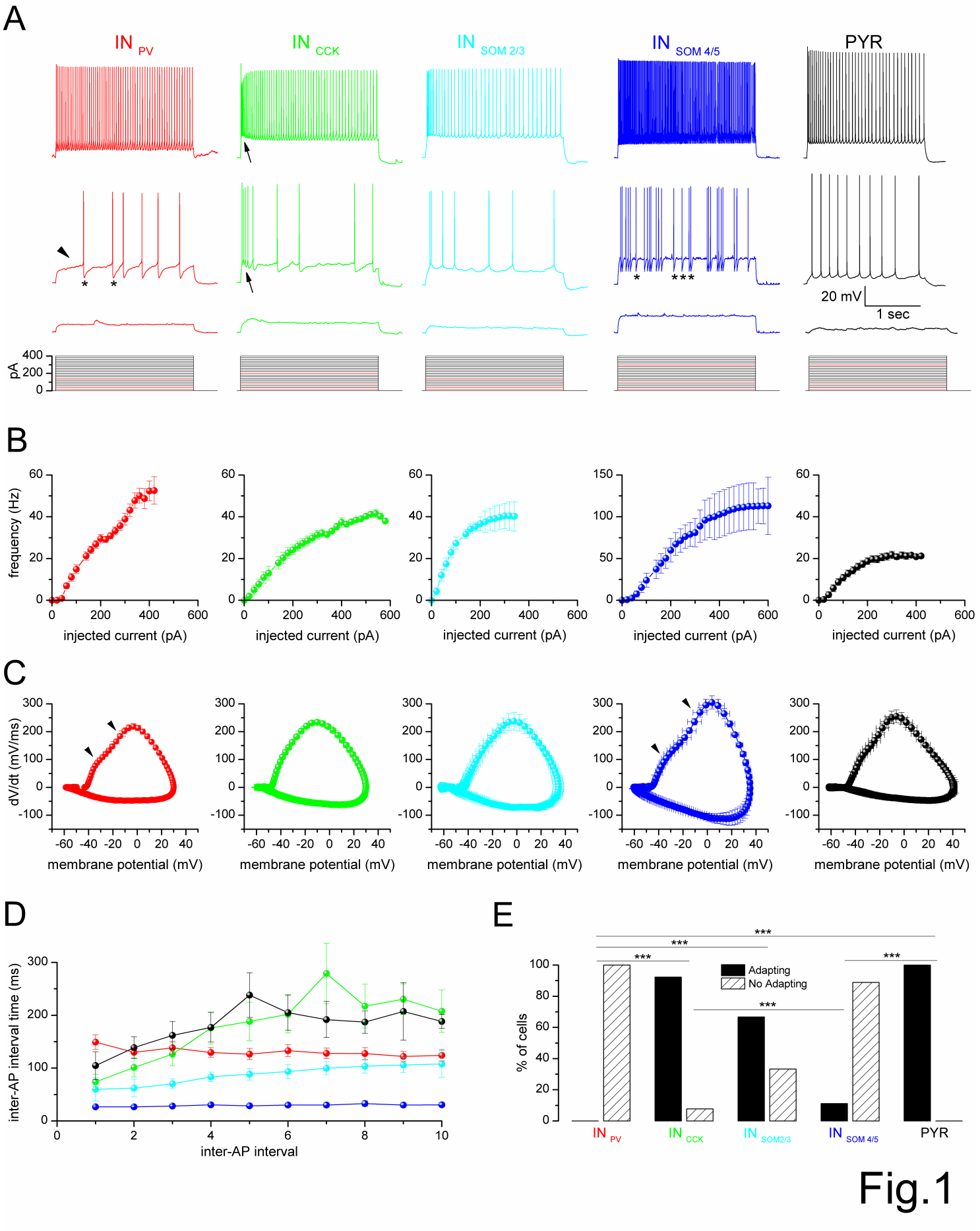
A
IN PV
IN CCK
IN SOM 2/3
IN SOM 4/5
PYR
20 mV
1 sec
pA
400
200
0
B
frequency (Hz)
injected current (pA)
C
dV/dt (mV/ms)
membrane potential (mV)
D
inter-AP interval time (ms)
inter-AP interval
E
% of cells
Adapting
No Adapting
***
IN PV
IN CCK
IN SOM2/3
IN SOM 4/5
PYR

Fig.1

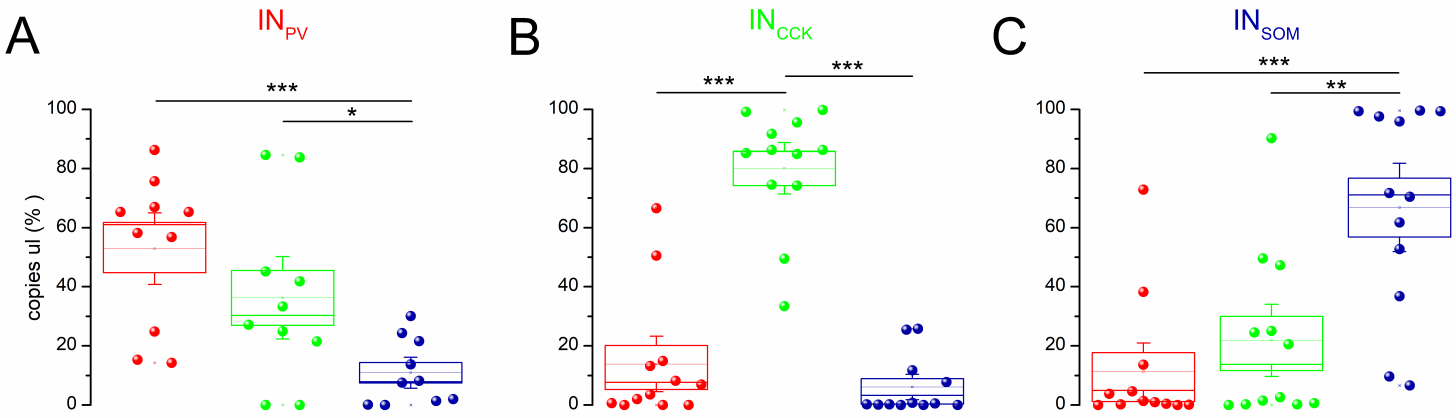

Fig.2

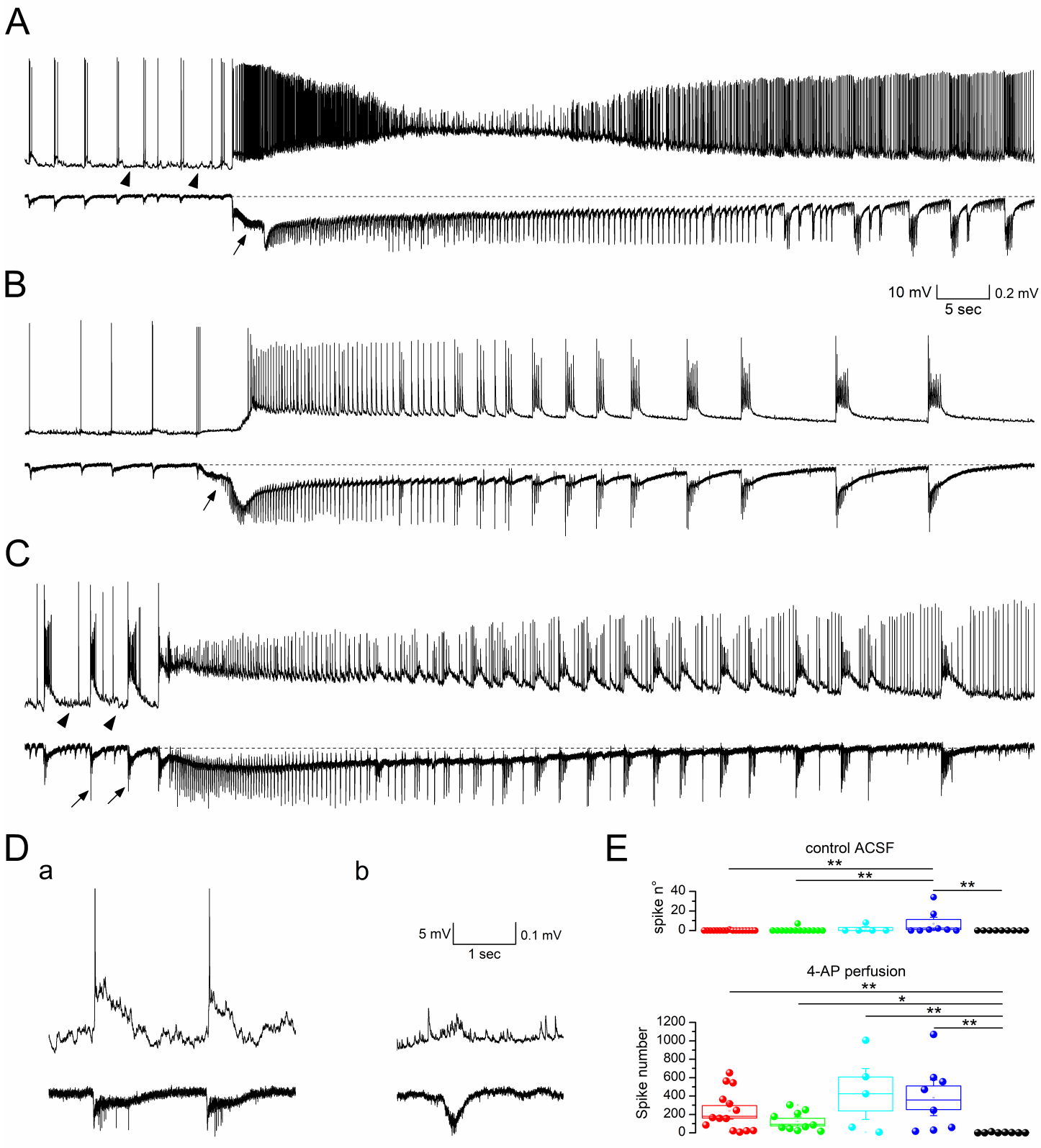
A
B
10 mV
0.2 mV
5 sec
C
D
a
b
5 mV
0.1 mV
1 sec
E
control ACSF
spike n°
40
20
0
**
**
**
4-AP perfusion
Spike number
1200
1000
800
600
400
200
0
**
*
**
**

Fig.3

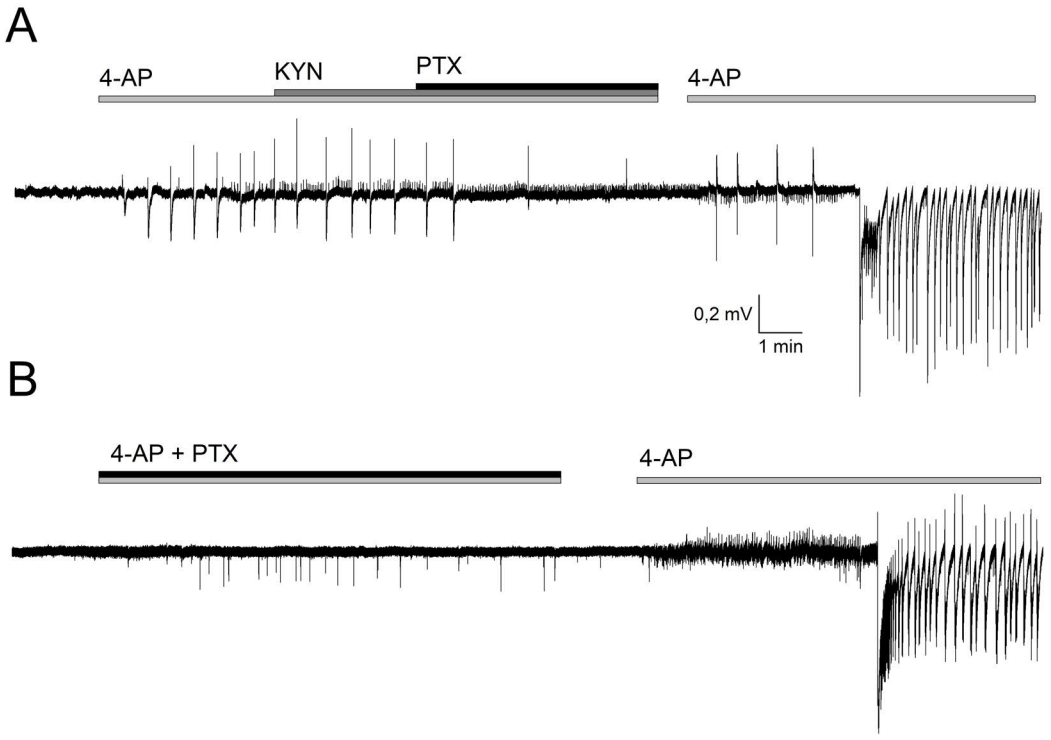
A
4-AP
KYN
PTX
4-AP
0,2 mV
1 min
B
4-AP + PTX
4-AP

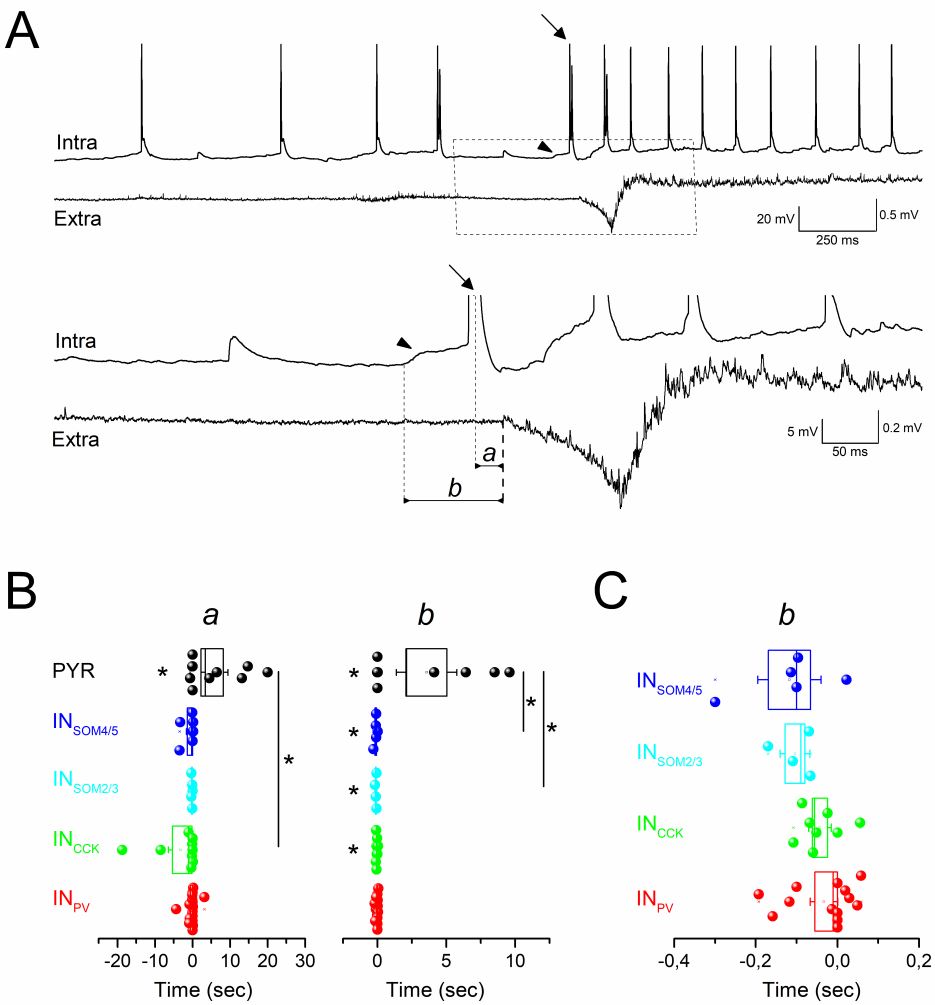
A
Intra
Extra
20 mV
0.5 mV
250 ms
Intra
Extra
5 mV
0.2 mV
50 ms
a
b
B
a
b
PYR
IN SOM4/5
IN SOM2/3
IN CCK
IN PV
-20 -10 0 10 20 30
Time (sec)
0 5 10
Time (sec)
C
b
IN SOM4/5
IN SOM2/3
IN CCK
IN PV
-0,4 -0,2 0,0 0,2
Time (sec)

Fig5

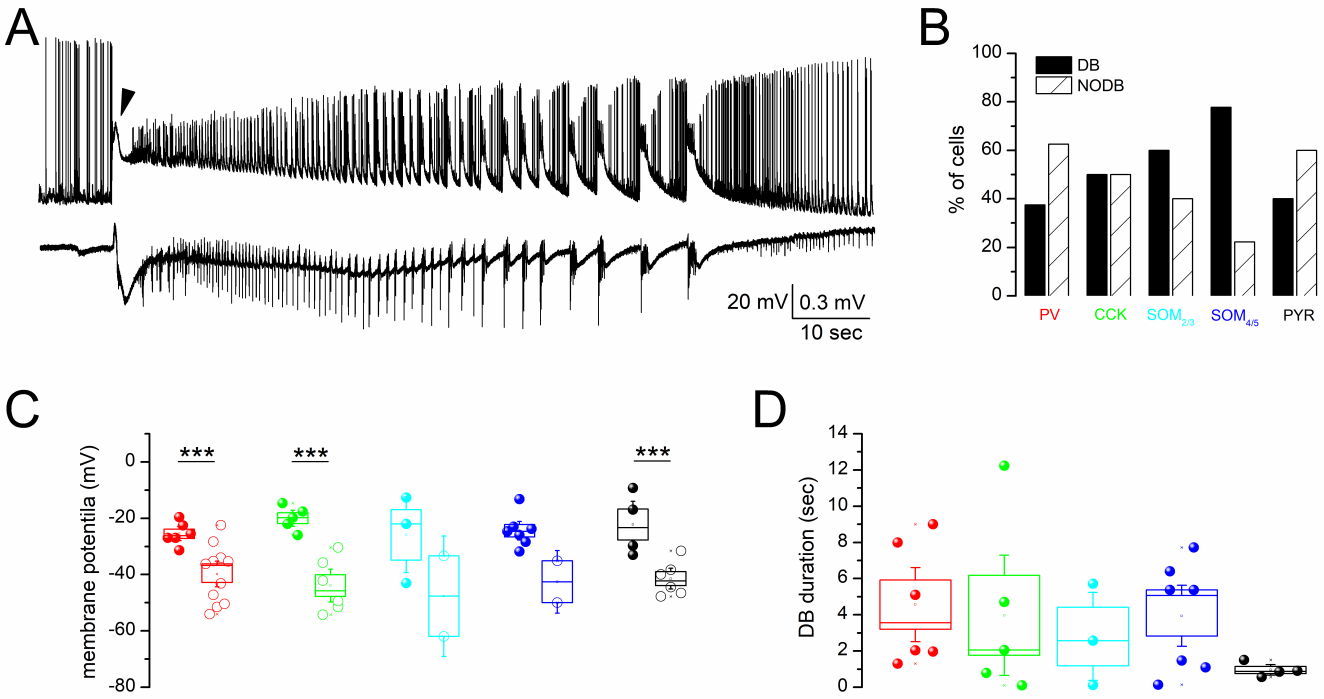
A
20 mV
0.3 mV
10 sec
B
DB
NODB
% of cells
100
80
60
40
20
0
PV
CCK
SOM2/3
SOM4/5
PYR
C
membrane potentila (mV)
0
-20
-40
-60
-80
***
***
***
D
DB duration (sec)
14
12
10
8
6
4
2
0

Fig.6

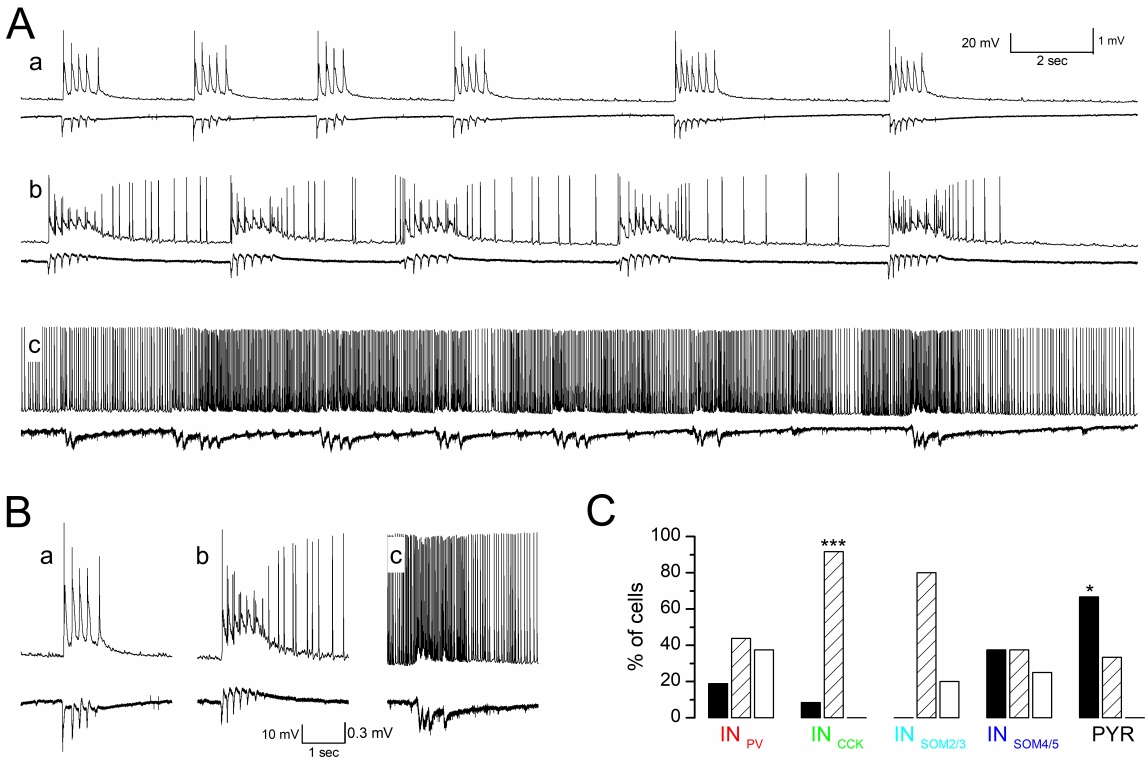
A
a
b
c
20 mV
1 mV
2 sec
B
a
b
c
10 mV
0.3 mV
1 sec
C
% of cells
100
80
60
40
20
0
***
*
IN PV
IN CCK
IN SOM2/3
IN SOM4/5
PYR

Fig.7